Geoscience Frontiers 17 (2026) 102328

Contents lists available at ScienceDirect

Geoscience Frontiers

journal homepage: www.elsevier.com/locate/gsf

Research Paper

Detrital zircon U-Pb-Hf isotopes redefine sedimentary continuity and crustal growth in the southern Mount Isa Inlier, North Australian Craton

Sutthida Noptalung *, Ioan V. Sanislav, Helen A. Cocker, Avish A. Kumar

Economic Geology Research Centre (EGRU) and Earth and Environmental Science, James Cook University, Townsville 4811, QLD, Australia

ARTICLE INFO

Article history:
Received 10 December 2025
Revised 10 March 2026
Accepted 7 April 2026
Available online 9 April 2026

Keywords:
Detrital zircon
Mount Isa Inlier
North Australian Craton
U-Pb dating
Lu-Hf isotopes
Crustal evolution

ABSTRACT

Detrital zircon U-Pb-Hf isotopic analysis was applied to metasedimentary rocks from the Dajarra region, southern Western Succession of the Mount Isa Inlier, to constrain maximum depositional ages (MDAs), provenance, and crustal evolution. Twelve samples from key stratigraphic units were analysed, including the Mount Guide Quartzite, Eastern Creek Volcanics, Jayah Creek Metabasalt, Timothy Creek Sandstone, Warrina Park Quartzite, Moondarra Siltstone, and Kallala Quartzite. MDAs vary significantly from those of units mapped as stratigraphic equivalents in the northern Western Succession. The Mount Guide Quartzite yields MDAs of 1883 ± 7 Ma and 1842 ± 9 Ma, substantially older than previously reported from the northern inlier. Metasedimentary units intercalated with the Eastern Creek Volcanics yield contrasting MDAs of 1877 ± 8 Ma and 1766 ± 15 Ma, indicating stratigraphic and depositional heterogeneity. The Jayah Creek Metabasalt contains interbedded quartzite with an MDA of 1857 ± 5 Ma, whereas the overlying Timothy Creek Sandstone yields an MDA of 1781 ± 15 Ma, consistent with an angular unconformity. The Warrina Park Quartzite and associated volcaniclastic units yield MDAs at 1862 ± 9 Ma, 1812 ± 5 Ma and 1781 ± 10 Ma, and the Moondarra Siltstone yields an MDA of 1776 ± 6 Ma. The Kallala Quartzite yields MDAs of 1812 ± 8 Ma and 1850 ± 4 Ma, indicating it is unlikely to form part of the Pre-Barramundi basement. Detrital zircons are dominated by late Paleoproterozoic populations with minor Neoarchean contributions. Zircon $\varepsilon_{Hf}(t)$ values range mainly between –6.7 and +8.7 and cluster near CHUR, indicating derivation from variably depleted to enriched crustal reservoirs consistent with mixed mantle-derived and evolved crustal source components. The combined U-Pb and Hf isotopic evidence challenges existing stratigraphic correlations and supports sediment derivation from mixed reworked crustal and juvenile sources within a subduction-related active continental margin during the late Paleoproterozoic. These results require revision of regional stratigraphic models and provide new constraints on basin evolution and crustal growth in the southern North Australian Craton.

1. Introduction

Detrital zircons from sedimentary and metasedimentary rocks are crucial for sedimentary provenance analysis and for understanding the formation and evolution of continental crust (Cawood et al., 2007; Hawkesworth et al., 2010; Lancaster et al., 2011; Gehrels, 2014). The integration of U-Pb dating with Hf isotope analysis provides a robust approach to constraining both the provenance and depositional ages of sediments, while also identifying their potential sources and tracking the processes involved in continental crustal growth and reworking (Zhang et al., 2014; Sanislav et al., 2018; Tomson and Amal Dev, 2024). Combined U-Pb ages and Hf isotopic compositions enable distinction between zircons derived from reworked older crust and those sourced from juvenile mantle-derived material, thereby allowing reconstruction of ancient tectonic and geodynamic settings (Hawkesworth and Kemp, 2006; Wang et al., 2013; Kohanpour et al., 2019). Furthermore, the age distributions of detrital zircons and their isotopic signatures can also be used to discuss the tectonic settings that formed the basins in which these sediments were deposited (Cawood et al., 2012; Barham et al., 2022).

The North Australian Craton (NAC) records a protracted history of volcano-sedimentary basin evolution during late Paleoproterozoic and early Mesoproterozoic with the most extensive successions preserved in the Mount Isa Inlier (de Vries et al., 2008).

* Corresponding author.
E-mail addresses: sutthida.noptalung@my.jcu.edu.au (S. Noptalung), ioan.sanislav@jcu.edu.au (I.V. Sanislav), helen.mccoywest@jcu.edu.au (H.A. Cocker), avish.kumar@jcu.edu.au (A.A. Kumar).

https://doi.org/10.1016/j.gsf.2026.102328

These thick volcano-sedimentary sequences are grouped into three major superbasins: the Leichhardt, Calvert, and Isa Superbasins (Fig. 1; Gibson et al., 2016). Their spatial and temporal relationships have been constrained through geological mapping (Blake, 1987), U-Pb geochronology (e.g., Page and Sweet, 1998; Southgate et al., 2000; Neumann et al., 2006) and geophysics surveys (e.g., Spampinato et al., 2015; Gibson et al., 2016). However, the tectonic settings associated with the formation of these basins remain debated, with models ranging from intracontinental rifting (Blake, 1980; Betts et al. 1998) to far-field back-arc setting along a continental margin (Giles et al., 2002; de Vries et al., 2008; Gibson et al., 2025). These interpretations are largely based on temporal correlations of the stratigraphic framework between the Mount Isa Inlier and other Proterozoic terranes within the NAC. Despite ongoing research, detailed geochronological and isotopic studies that directly constrain the evolution of these sedimentary basins and their tectonic settings in the Mount Isa region remain limited, leading to significant uncertainty regarding the timing, provenance, and tectonic evolution of these superbasins.

This study integrates U-Pb geochronology and Lu-Hf isotopic analyses of detrital zircons from the Dajarra region located in the southern part of the Western Succession (WS) of the Mount Isa Inlier. The results help constrain the maximum depositional ages, sediment provenance, and source characteristics of the major stratigraphic units from this part of the inlier and provide the basis for regional stratigraphic correlations. The results are further discussed in terms of crustal evolution and the tectonic setting of sedimentary basins within the Mount Isa Inlier, with broader implications for evolution across the NAC during the Paleoproterozoic.

2. Regional geologic and stratigraphic framework

The Mount Isa Inlier is located on the eastern part of the NAC (Fig. 1a) and preserves a protracted Paleoproterozoic to Mesoproterozoic evolution including multiple orogenic and basin forming events between ca. 1870 Ma and 1490 Ma (Blake and Stewart, 1992; MacCready et al., 1998; Scott et al., 2000; Betts et al., 2006; Spence et al., 2022). The Mount Isa Inlier was subdivided into three main tectonostratigraphic components, namely the Eastern Fold Belt (EFB), the Western Fold Belt (WFB) and the central Kalkadoon-Leichhardt Belt (KLB) (Fig. 1b). Furthermore, these

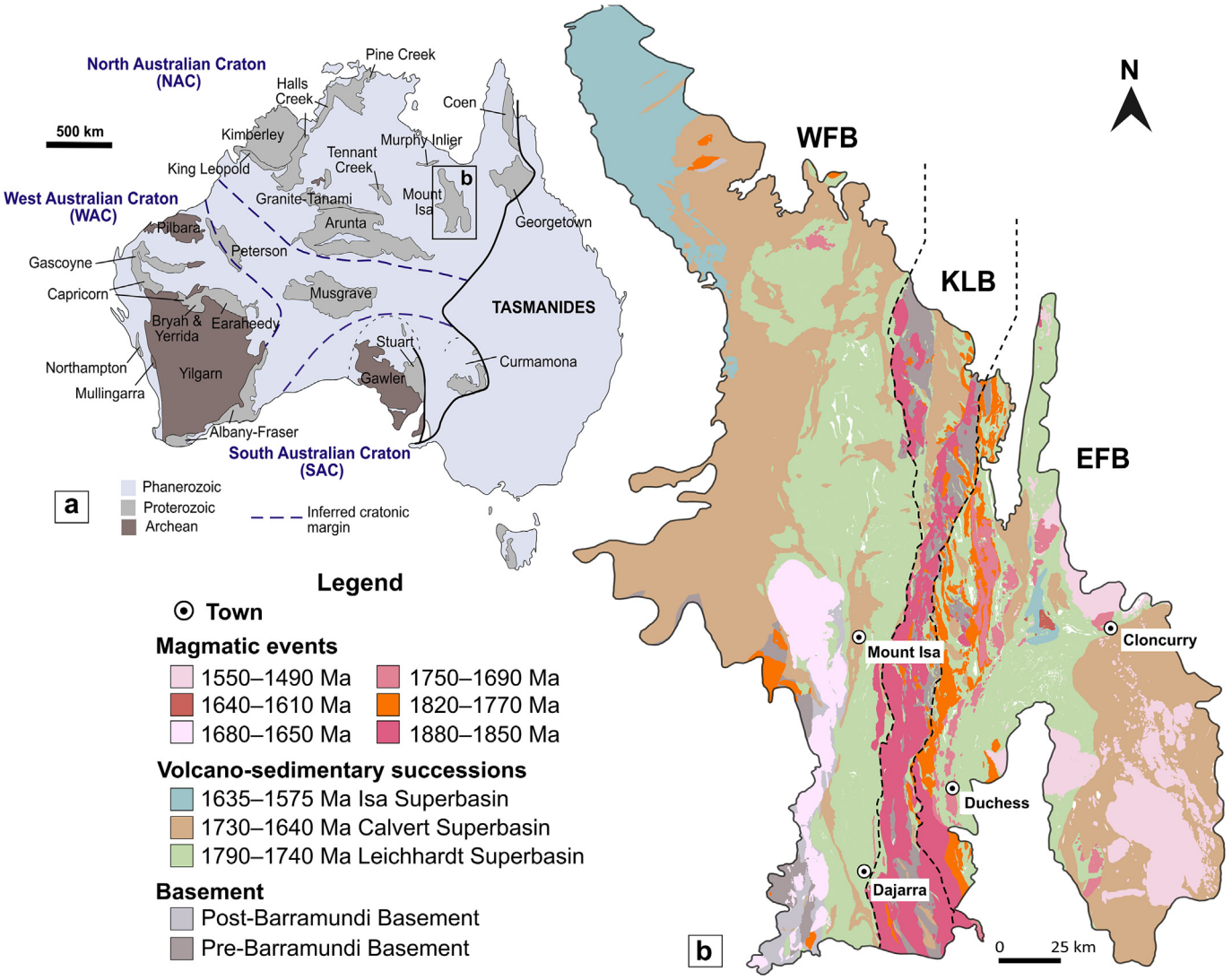

Fig. 1. Map of Australian continent showing the distribution of Proterozoic inliers, including Mount Isa Inlier located in the North Australian Craton (NAC) (a). Simplified geology of Mount Isa Inlier showing the distribution of basement rocks, volcano-sedimentary successions, and major magmatic events (b). The Mount Isa inlier can be divided into three domains: the Western Fold Belt (WFB), Kalkadoon-Leichhardt Belt (KLB), and Eastern Fold Belt (EFB).

three belts have been subdivided into N-S trending domains based on variations of their geological settings and the presence of bounding structures (Withnall and Hutton, 2013). Within the Mount Isa Inlier, a thick volcano-sedimentary succession (deposited between ca. 1800 Ma and 1575 Ma) overlies crystalline basement rocks, with their distribution and continuity broadly controlled by the orientation of regional structures (Fig. 1b). The stratigraphy of these volcano-sedimentary successions has been interpreted to be correlative across the inlier (Blake, 1980, 1986; Foster and Austin, 2008).

The study area forms part of the Paleoproterozoic NAC, which experienced significant tectono-magmatic event during the Barramundi Orogeny (ca. 1880–1840 Ma), a major crust-forming and reworking event that affected large portions of northern Australia. This orogenic episode provides an important regional framework for interpreting zircon age and Hf isotopic patterns discussed below. The crystalline basement rocks within the inlier, preserved in the KLB and the southern part of the WFB, has been mapped as Pre- and Post-Barramundi basement (Fig. 1b). Three rock units are recognized within the Pre-Barramundi basement: the Yaringa Metamorphics, the Saint Ronans Metamorphics, and the Sulieman Gneiss (Fig. 2). These rocks represent sedimentary sequences deposited before ca. 1870 Ma (Blake and Stewart, 1992) that were subsequently deformed and metamorphosed during the Barramundi Orogeny (Etheridge et al., 1987; Page, 1988; Page and Williams, 1988; Bierlein et al., 2008). The Barramundi Orogeny was broadly contemporaneous with the Kalkadoon Igneous Event (KIE) (Etheridge et al., 1987; Page, 1988; Page and Williams, 1988; Bierlein et al., 2008), with magmatic activity between ca. 1880 Ma and 1850 Ma constrained by crystallization ages of intrusive and extrusive units (Fig. 2). The Barramundi Orogeny was followed by the deposition of volcano-sedimentary sequences mapped as Post-Barramundi basement, although debate remains regarding the timing of their metamorphism and deformation, as well as their stratigraphic position (Withnall and Hutton, 2013). Post-Barramundi units include the Oroopo Metabasalt, Bucket Hole Metavolcanics, Kallala Quartzite, May Downs Gneiss and Alpha Centauri Metamorphics. These units are mainly exposed within the southwestern part of the Mount Isa Inlier and were previously assigned to the Haslingden Group (Blake et al., 1980, 1982, 1986) (Fig. 2). However, recent detrital zircon geochronology (e.g., Carson et al., 2009; Magee et al., 2012) constrains the maximum depositional ages of the Oroopo Metabasalts and Bucket Hole Metavolcanics to before ca. 1810 Ma. The onset of the Argylla Igneous Event has been interpreted as marking the termination of sedimentation prior to ca. 1810 Ma (Wyborn, 1988; Carson et al., 2011; Withnall and Hutton, 2013; Cocker et al., 2025).

The major volcano-sedimentary successions of the Mount Isa Inlier, deposited between ca. 1800 Ma and 1575 Ma, are referred to as the Western Succession (WS) in the Western Fold Belt (WFB) and the Eastern Succession (ES) in the Eastern Fold Belt (EFB). The stratigraphic framework of the inlier is complex, with lithological units that are broadly similar yet repeated at different stratigraphic levels. Traditionally, these successions were classified on the basis of regionally significant unconformities and grouped into a series of cover sequences (Blake, 1980, 1986; Blake and Stewart, 1992). More recently, the framework has been revised, with the cover sequences reassigned and integrated into a series of supersequences that collectively define three major superbasins: the Leichhardt, Calvert, and Isa Superbasins (Gibson et al., 2016).

The onset of sedimentary deposition in the Leichhardt Superbasin (ca. 1790–1740 Ma) is recorded in the WS by the Bottletree Formation, exposed in the eastern Leichhardt River domain (Fig. 2). This succession was overlain by siliciclastic deposits and bimodal volcanism of the Lower Haslingden Group, comprising the Mount Guide Quartzite and the Eastern Creek Volcanics (ECVs). The Mount Guide Quartzite, the basal unit of the Lower Haslingden Group, is particularly widespread in the eastern Leichhardt River domain and is interpreted as equivalent to the Leander Quartzite, a clastic sedimentary unit with more restricted exposure in the northern part of the domain. The overlying ECVs represent interbedded siliciclastic sediments and bimodal volcanic rocks, forming an extensive unit across both the Leichhardt River and Mount Oxide domains (Eriksson and Simpson, 1993). The ECVs consists mainly of mafic volcanics interbedded with minor amount of volcaniclastic and siliciclastic sediments. The older part consists of the Cromwell Metabasalt Member whereas the upper part consists of the Pickwick Metabasalt Member. These two mafic units are separated by the intervening Lena Quartzite. Similar mafic units metamorphosed to amphibolite facies in the southern Leichhardt River domain were mapped as the Jayah Creek Metabasalt and interpreted to be equivalent to the ECVs (Blake, 1980, 1984, 1986; Bultitude, 1982). In the ES, temporally equivalent bimodal volcanic units include the Magna Lynn Metabasalt and the Argylla Formation (Foster and Austin, 2008) together with the volcano-sedimentary rocks of the Boomarra Horst in the Mitakoodi domain. The Boomarra Horst is in turn overlain by felsic volcanic rocks of the Bulonga and Marraba Volcanics. Following this phase of extensive bimodal volcanism, deposition in the WS became dominated by siliciclastic sedimentation, represented by the Myally Subgroup which represents the uppermost part of the Haslingden Group. The deposition of the Haslingden Group was succeeded by siliciclastic and calcareous deposits of the Quilalar Formation, which is interpreted to be stratigraphically equivalent to the Ballara Quartzite and the Corella Formation in the Kalkadoon-Leichhardt and Mary Kathleen domains (Foster and Austin, 2008).

The accumulation of volcano sedimentary successions during the Calvert Superbasin (ca. 1730–1640 Ma) in the WS commenced (Fig. 2) with depositions of the Bigie Formation and the bimodal Fiery Creek Volcanics at ca. 1710 Ma (Page and Sweet, 1998; Neumann et al., 2006). These units are mainly exposed in the central to northern parts of the Leichhardt River and Mount Oxide domains and are unconformably overlain by the Surprise Creek Formation (Blake, 1987). This was followed by the extensive deposition of the Mount Isa and McNamara Groups. The Mount Isa Group comprises the Warrina Park Quartzite, Moondarra Siltstone, Breakaway Shale, Native Bee Siltstone, Urquhart Shale, Spear Siltstone, Kennedy Siltstone, and Magazine Shale. The Warrina Park Quartzite and Moondarra Siltstone, assigned as the basal units of the Mount Isa Group, accumulated between ca. 1690 Ma and 1670 Ma in the central to northern Leichhardt River domain (Jackson et al., 2005; Neumann et al., 2009b). These formations were also mapped by Bultitude (1982) and Blake (1987) to occur in the southern part of the Leichhardt River domain. The remainder of the Mount Isa Group was deposited after ca. 1670 Ma, predominantly within the central to northern Leichhardt River domain. Sedimentary deposition of the McNamara Group occurred broadly coeval with the Mount Isa Group and has been interpreted as a correlative succession. The McNamara Group is extensive in the Mount Oxide domain and further distributed into the Century and Camooweal-Murphy domains (Domagala et al., 2000; Krassay et al., 2000; Page et al., 2000). Beyond the WS, supersequences within the Calvert Superbasin are less extensively preserved in the Kalkadoon-Leichhardt and Mary Kathleen domains. In contrast, the volcano-sedimentary units are more widespread within the Marimo-Staveley, Kuridala-Selwyn, Doherty-Fig Tree Gully, and Soldiers Cap domains, where their depositional ages are constrained between ca. 1675 Ma and 1650 Ma (Foster and Austin, 2008).

The volcano-sedimentary successions of the Isa Superbasin are comparatively less extensive within the Mount Isa Inlier (Fig. 2).

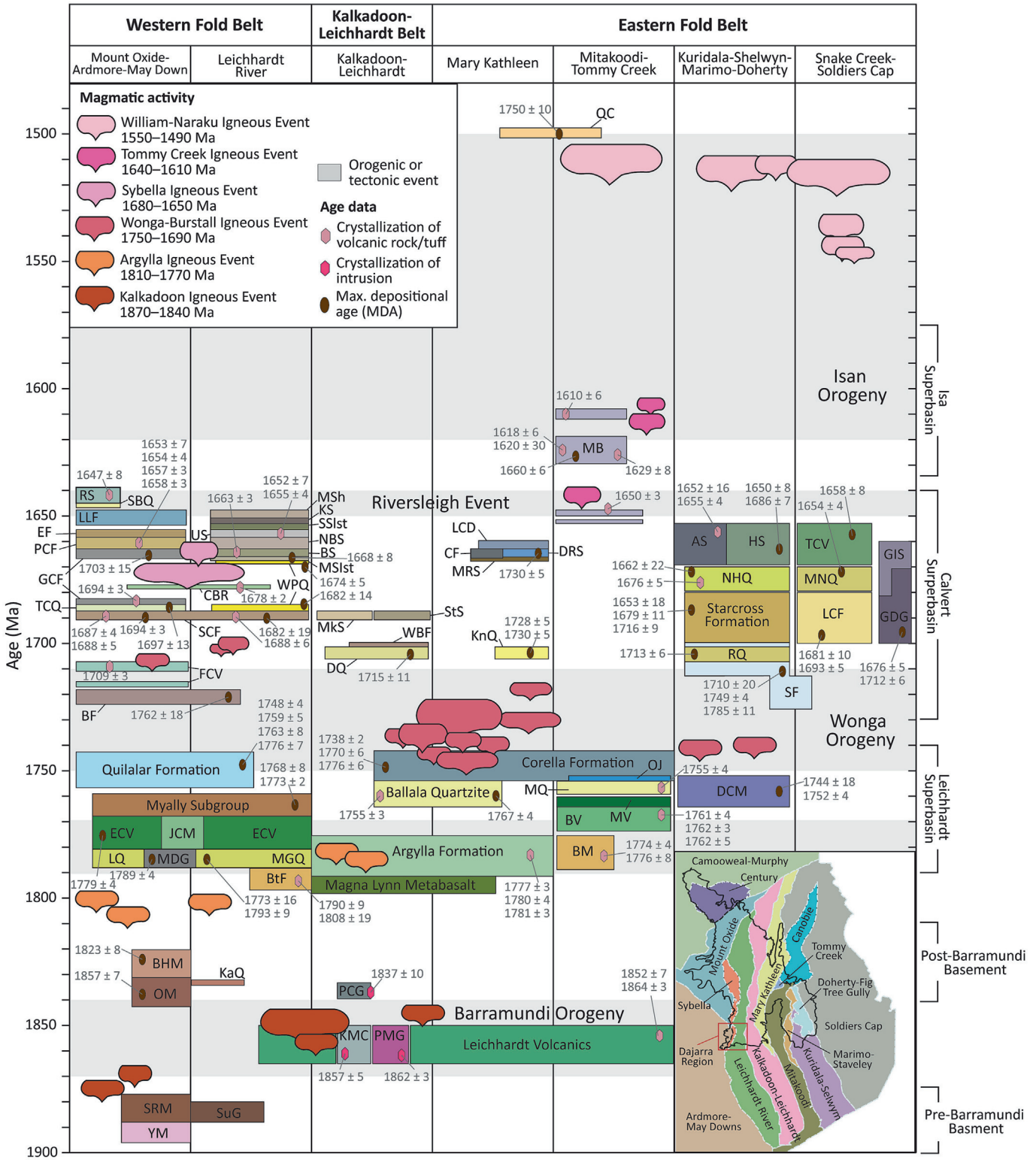

Fig. 2. Time-space chart of the stratigraphic successions in the Mount Isa Inlier, modified after Foster and Austin, (2008) and Olierook et al. (2022). Domain boundaries after Geological Survey of Queensland (2011). Unit abbreviations: AS = Answer Slate, BHM = Bucket Hole Metavolcanics, BF = Bigie Formation, BM = Boomarra Metamorphics, BS = Breakaway Shale, BtF = Bottletree Formation, BV = Bulonga Volcanics, CBR = Caters Bore Rhyolite, CF = Coocerina Formation, DCM = Double Crossing Metamorphics, DQ = Deighton Quartzite, DRS = Dugald River Shale, ECV = Eastern Creek Volcanics, EF = Esparanza Formation, FCV = Fiery Creek Volcanics, GCF = Gunpowder Creek Formation, GDG = Gandry Dam Gneiss, GIS = Glen Idol Schist, HS = Hampden Slate, JCM = Jayah Creek Metabasalt, KaQ = Kallala Quartzite, KMC = Kurbayia Metamorphic Complex, KnQ = Knapdale Quartzite, KS = Kennedy Siltstone, LCD = Lady Clayre Dolomite, LCF = Llewellyn Creek Formation, LLF = Lady Loretta Formation, LQ = Leander Quartzite, MB = Milo Bed, MDG = May Downs Gneiss, MGQ = Mount Guide Quartzite, MkS = Makbhat Sandstone, MNQ = Mount Norma Quartzite, MQ = Mitakoodi Quartzite, MRS = Mt Roseby Schist, MSh = Magazine Shale, MSlst = Moondarra Siltstone, MV = Marraba Volcanics, NBS = Native Bee Siltstone, NHQ = New Hope Quartzite, OM = Oroopo Metabasalt, OJ = Overhang Jaspilite, PCF = Paradise Creek Formation, PCG = Pothole Creek Gneiss, PMG = Plum Mountain Gneiss, QC = Quamby Conglomerate, RQ = Roxmere Quartzite, RS = Riversleigh Siltstone, SBQ = Shady Bore Quartzite, SCF = Surprise Creek Formation, SF = Staveley Formation, SRM = Saint Ronans Metamorphics, SSlst = Spear Siltstone, StS = Stanbroke Sandstone, SuG = Sulieman Gneiss, US = Urquhart Shale, TCQ = Torpedo Creek Quartzite, TCV = Toole Creek Volcanics, WBF = White Blow Formation, WPQ = Warrina Park Quartzite, YM = Yaringa Metamorphics.

In the Tommy Creek domain, sedimentary units have been correlated with the Isa Superbasin on the basis of maximum depositional ages reported by Brown et al. (2023). By contrast, the Isa Superbasin is most extensively developed in the Century and Camooweal-Murphy domains, with further distribution to the northwest where it is also preserved in the Murphy Inlier (Bradshaw et al., 2000). Regionally, this succession is represented by the upper part of the McNamara Group, which has been constrained to have accumulated between ca. 1630 Ma and 1585 Ma (Page et al., 2000; Southgate et al., 2000).

The evolution of the three superbasins was interpreted to be coeval with significant magmatism (Fig. 2) including the Argylla Igneous Event (AIE), the Wonga-Burstall Igneous Event (WBIE), and the Sybella Igneous Event (SIE) (Wyborn et al., 1988; Neumann et al., 2006, 2009a; Bultitude et al., 2021; Cocker et al., 2025). Furthermore, previous studies interpreted that the basin-forming events represent episodes of continental rifting in a back-arc setting of a complex subduction system occurring either along the southern or the eastern margin of NAC (Blake and Stewart, 1992; Page and Sweet, 1998; Scott et al., 2000; Giles et al., 2002; Foster and Austin, 2008; Iaccheri, 2019).

Two more orogenic events were suggested to have affected the Mount Isa Inlier, the 1750–1710 Ma Wonga Orogeny (Spence et al., 2021, 2022) and the 1650–1490 Ma Isan Orogeny (O'Dea et al., 1997b; MacCready et al., 1998; Abu Sharib and Sanislav, 2013) (Fig. 2). A compressive event between ca. 1800 Ma and 1770 Ma was documented from the Tick Hill region, but the full extent and its regional significance is not yet known (Le et al., 2021a, 2024). The onset of the Wonga Orogeny coincides with the cessation of sedimentation during the Leichhardt Superbasin, and it appears that the deformation and metamorphism during this orogenic event was most intense in the EFB (Wilson, 1975; Betts, 1999; Blaikie et al., 2017; Spence et al., 2021, 2022). In the WS, the Isan Orogeny may have initiated with the 1650–1640 Ma Riversleigh Event marking the cessation of sedimentation during the Calvert Superbasin (Gibson et al., 2016, 2020). The Isan Orogeny affected the entire inlier and resulted in the reactivation of previous structures and the cessation of sedimentation in the region (Blake and Stewart, 1992; Connors and Page, 1995; O'Dea et al., 1997b; Abu Sharib and Sanislav, 2013; Gibson et al., 2016). The final stages of the Isan Orogeny coincide with the emplacement of voluminous I-type magmatism with A-Type affinities, the Williams Igneous Event, in the EFB between ca. 1550–1490 Ma (Wyborn, 1998).

2.1. Geology and stratigraphy of the Dajarra region

The Dajarra region, located in the southwestern part of the Mount Isa Inlier, comprises four distinct geological domains arranged from west to east: the Ardmore-May Downs domain, the Sybella domain, the Leichhardt River domain, and the Kalkadoon-Leichhardt domain (Fig. 2). The eastern boundary of the Dajarra region is defined by the Dajarra Fault within the Kalkadoon-Leichhardt domain (Fig. 3). The Ardmore-May Downs domain is dominated by Pre- and Post- Barramundi basement rocks, whereas the Leichhardt River and Kalkadoon-Leichhardt domains are largely composed of the Bottletree Formation, the Lower Haslingden Group and the basal formations of the Mount Isa Group (Fig. 3). The region preserves a complex history of sedimentation, deformation, magmatism and metamorphism. The Pre-Barramundi basement rocks are represented by the Sulieman Gneiss and Saint Ronan Metamorphics in the western part and by the Leichhardt Volcanics and the Kurbayia Metamorphics. The Post-Barramundi basement rocks occur only in the western part of the region, was deformed and metamorphosed from greenschist to amphibolite facies (Blake et al., 1982), and consist of the Oroopo Metabasalt, Bucket Hole Metavolcanics, Alpha Centauri Metamorphics and Kallala Quartzite.

The oldest metasedimentary unit of the Leichhardt Superbasin in the Dajarra region is the Bottletree Formation. This unit is overlain by the Lower Haslingden Group consisting of the Yappo Member, Mount Guide Quartzite, ECVs, Jayah Creek Metabasalt and Timothy Creek Sandstone. These successions are interpreted to represent syn-rift volcanism and rift-related sedimentation deposited in a fluvial to lacustrine environments (Jackson et al., 2000; Neumann et al., 2006). The Bottletree Formation and the Haslingden Group are mapped as continuous units that extend for more than 700 km from the northern part of the inlier to the southernmost margin of the inlier, extending undercover until the Cork Fault (e.g. Spampinato et al., 2015). Notably, the succession substantially thickens in the Dajarra region relative to the northern part of the inlier (Blake et al., 1982; Bultitude, 1982; Spampinato et al., 2015; Olierook et al., 2022). Units such as the Myally Subgroup, Quilalar Formation and equivalents that are widespread in the northern part of the WS are missing from Dajarra region. Also, units belonging to the Bigie Formation, Fiery Creek Volcanics and Surprise Creek Formation or equivalents are missing from the Dajarra Region. The only sedimentary units of the Calvert Superbasin found in the Dajarra region are assigned to the Warrina Park Quartzite and Moondarra Siltstone, which occur as a narrow north–south trending belt enclosed by the Haslingden Group rocks on both sides. They are interpreted to reflect marine siliciclastic deposition ranging from shoreface to shallow-marine settings and have been metamorphosed to lower greenschist facies. No Isa Superbasin sediments have been identified in the Dajarra region.

At least four intrusive events are recorded in the Dajarra region: the KIE, the AIE, the WBIE, and the SIE (Fig. 3). Most intrusions within the Ardmore-May Downs and Sybella domains are attributed to the SIE, represented by plutons of various sizes that intrude the basement rocks. However, some intrusions in these domains are assigned to the AIE (Carson et al., 2009, 2011), emplaced within units mapped as basement rocks as well as within the Jayah Creek Metabasalt. In the Kalkadoon-Leichhardt domain, the AIE is represented by a small pluton intruding the basement units (Magee et al., 2012). By contrast, the voluminous plutonic bodies in the Kalkadoon-Leichhardt domain are assigned to the KIE, which likely intruded the Bottletree Formation. This formation is also intruded by a north–south trending granite, the Camel Creek Granite, which is mapped as part of the WBIE. Additionally, the Wonga-Burstall granitoids include the Garden Porphyry Dyke, a long, narrow, north–south trending porphyritic intrusion emplaced within the Mount Guide Quartzite. However, Noptalung et al. (2026) revised the magmatic emplacements ages, units classification and mapped distribution of all intrusive rocks in the Dajarra region.

3. Methodology

3.1. Sampling and analytical methods

This study is based on samples collected from metasedimentary units cropping out in the Dajarra region for zircon U-Pb geochronology and Lu-Hf isotope studies. The sampling strategy focused on major units that had not previously been dated (Fig. 4).

Detrital zircon separation was carried out at James Cook University, Townsville. Zircon grains were extracted from crushed rock samples using a Wilfley table, handpicked under a binocular microscope, and mounted in epoxy resin. The mounts were polished to expose grain interiors, carbon-coated, and imaged using cathodoluminescence (CL) with a Hitachi SU5000 FE-SEM at the Advanced Analytical Centre (AAC), James Cook University, to char-

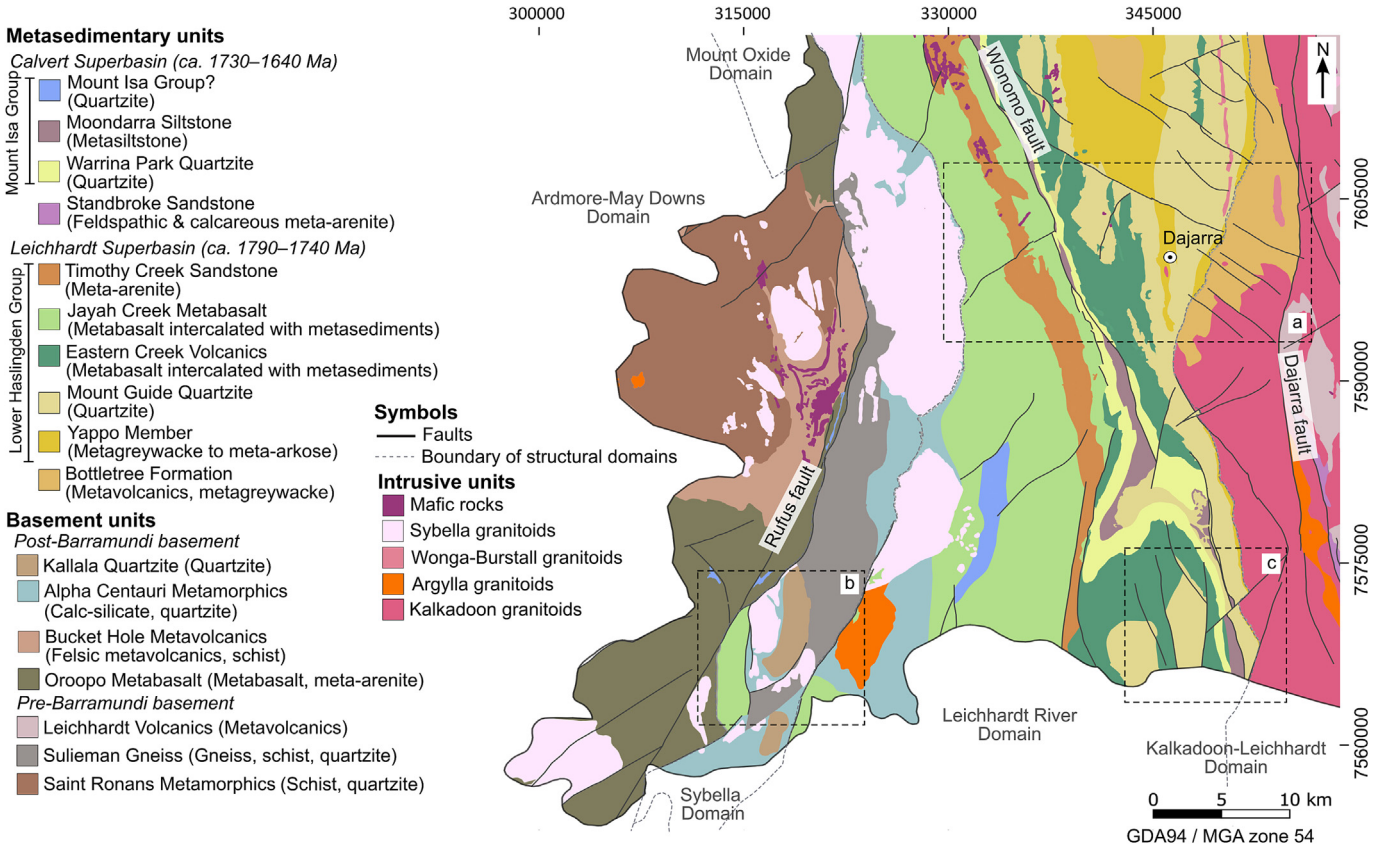

Fig. 3. Geological map of Dajarra region showing the distribution of the main geological units. The areas highlighted with dashed lines indicate more detailed maps illustrated in Fig. 4.

acterise internal compositional domains. Zircon internal textures observed in the CL images were used to guide the selection of U-Pb analytical spots, preferentially targeting oscillatory growth zones and avoiding domains showing evidence of metamorphic overgrowth. U-Pb zircon geochronology was carried out at the AAC using laser ablation-inductively coupled plasma mass spectrometry (LA-ICP-MS). Analyses were performed with a Thermo Scientific iCAP RQ-ICP-MS coupled to a Teledyne Photon Machines Analyte G2 excimer laser system. Each analytical session started with 30 s blank gas measurement, followed by a 30 s ablation period using a spot size of 25 or 30 μm at a fluence of 3 J/cm^2 and 5 Hz repetition rate. Each analytical run included 10 analyses of unknown zircons, bracketed by one analysis of international glass standard NIST610, two analyses of the primary reference zircon standard GJ-1 (LA-ICP-MS $^{206}Pb/^{238}U$ age of 601.86 ± 0.37 Ma; Horstwood et al., 2016) and two analyses of secondary reference zircon standards FC1 (TIMS $^{207}Pb/^{206}Pb$ age of 1099.0 ± 0.6 Ma; Paces and Miller Jr., 1993) and Temora-2 (IDTIMS $^{206}Pb/^{238}U$ age of 416.8 ± 0.3 Ma; Black et al., 2003; Tichomirowa et al., 2019). The primary reference standard was used to correct for mass bias, instrumental drift, and down-hole fractionation in isotope ratios. The secondary standards provided an independent assessment of accuracy and precision, while the glass standard monitored instrumental stability. Data reductions were performed using the Iolite software package (Paton et al., 2011). The average measured ages of the reference zircons were 601.89 ± 1.14 Ma for GJ-1, 1094.5 ± 8.2 Ma for FC-1, and 416.6 ± 1.8 Ma for Temora-2. The detrital zircon data were subsequently visualized using IsoplotR (Vermeesch, 2018). For age determination, the $^{207}Pb/^{206}Pb$ age was used. Maximum depositional ages (MDAs) were determined using both the weighted mean age of the youngest population and the Maximum Likelihood Algorithm (MLA), with results reported at the 95% confidence level based on analyses exhibiting less than 10% discordance. Pb loss and metamorphic disturbance typically produce discordant U-Pb systematics in zircon and can generate an apparent young tail in detrital age spectra. To mitigate this effect, depositional interpretations are based exclusively on analyses within a ± 10% discordance threshold and on $^{207}Pb/^{206}Pb$ ages, which are less sensitive than $^{206}Pb/^{238}U$ ages to modest Pb loss at Paleoproterozoic ages. Nevertheless, we recognise that where discordance is pervasive and only a small subset of grains remains after filtering, the concordant population may be less representative of the original detrital assemblage (e.g., preferential survival of less-damaged grains or mixed-domain ablation). Accordingly, MDAs from samples with very low proportions of concordant analyses or small youngest clusters are treated conservatively as maximum constraints. Probability density plots (PDPs) were generated using kernel density estimation with a histogram bin size of 15 Myr. Detrital zircon age spectra provide insights into temporal distribution and provenance of detritus. Beyond serving as provenance tracers, detrital ages spectra can also be used to infer tectonic settings, based om the hypothesized relationship between detrital zircon age distributions and geodynamic settings (Cawood et al., 2012; Barham et al., 2022). Cumulative age distribution (CAD) plots and related detrital zircon discrimination approaches provide probabilistic insights into basin type and tectonic setting but are not uniquely diagnostic. Age distributions may overlap between tectonic environments, and their interpretative strength increases where coeval igneous sources are independently identified and temporally constrained within the region. Accordingly, CAD-

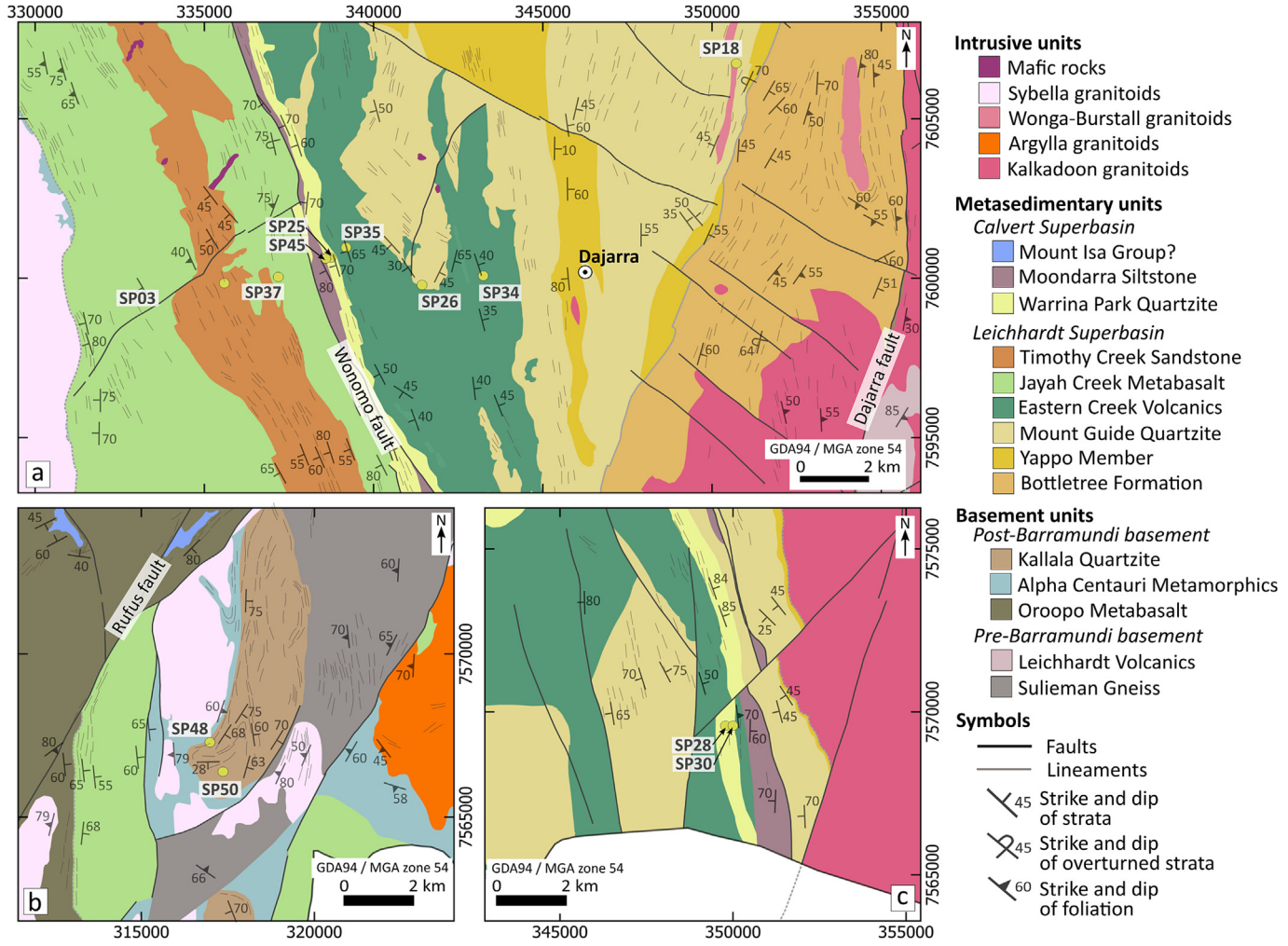

Fig. 4. Detailed geological maps for the selected areas showing the geological context of samples used in this study.

based interpretations in this study are integrated with regional magmatic history, Hf isotopic signatures, and stratigraphic relationships rather than used as standalone tectonic indicators.

Lu-Hf isotope analyses followed the analytical procedures established at the AAC (Kemp et al., 2009; Sanislav et al., 2014). The analyses were conducted on zircon grains that had previously undergone U-Pb dating, using a Thermo Scientific Neptune MC-ICP-MS coupled with a Teledyne Photon Machines Analyte G2 laser ablation system. The laser was operated at a frequency of 4 Hz with a beam diameter of 50 μm. The accuracy of results was monitored using the reference zircon standard Mud Tank (MTZ), which was analysed alongside the unknown samples. The measured average $^{176}Hf/^{177}Hf$ value for MTZ during this session was 0.282491 ± 11 (2σ), while the accepted value of 0.282507 ± 6 (2σ) reported by Woodhead and Hergt (2005). A normalization factor of 1.000056 was calculated from this discrepancy and applied to the measured $^{176}Hf/^{177}Hf$ value of unknown samples and the reference zircon standard FC1. The FC1 zircon was used to assess the accuracy of isobaric interference corrections, particularly from Yb. Following normalization, the measured average $^{176}Hf/^{177}Hf$ value for FC1 Zircon (0.282182 ± 14; 2σ) was within analytical uncertainty with expected value of 0.282184 ± 16 (2σ) reported by Woodhead and Hergt (2005). Epsilon hafnium (ε_{Hf}) values were calculated using present-day chondritic uniform reservoir (CHUR) parameters: $^{176}Hf/^{177}Hf$ = 0.282785 and $^{176}Lu/^{177}Hf$ = 0.0336 (Bouvier et al., 2008). Initial $^{176}Hf/^{177}Hf$ ratios were determined using a ^{176}Lu decay constant of 1.867 × 10^{-5} Myr^{-1} (Söderlund et al., 2004).

3.2. Estimation of maximum depositional age

In this study, maximum depositional ages (MDAs) are determined using the Maximum Likelihood Age (MLA) method of Vermeesch (2021), which estimates the statistically youngest age mode within the detrital zircon population while explicitly incorporating individual analytical uncertainties. The youngest population is identified from analyses within ± 10% discordance and evaluated for coherence using MSWD and overlap at 2σ uncertainty. Weighted mean $^{207}Pb/^{206}Pb$ ages of the youngest overlapping grain clusters were calculated as an independent verification following Spencer et al. (2016); however, depositional interpretations are based primarily on MLA-derived ages to minimise subjectivity in cluster selection and to better accommodate sparse or partially dispersed youngest grains.

The MLA approach formally assumes that the age distribution can be approximated by a mixture of a youngest population and an older background population. Although natural detrital zircon samples typically record more complex multi-source histories, MLA is applied here pragmatically to isolate the statistically youngest coherent age component rather than to model the full age distribution. As with all MDA methods, pervasive Pb-loss or

mixed-domain ablation may influence the youngest tail; therefore, MLA-derived ages are interpreted conservatively and evaluated alongside concordance filtering and weighted mean results to ensure geological plausibility.

To ensure transparency in the interpretation of MDAs, the youngest zircon population in each sample was defined using the following criteria: (1) analyses must exhibit < 10% discordance; (2) the youngest cluster must consist of at least three concordant grains that overlap at 2σ uncertainty; and (3) the cluster must form a statistically coherent group with MSWD ≤ 2.0. Where more than one coherent young cluster was present, the youngest statistically robust population was selected.

MDAs are considered to approximate true depositional age only when the youngest population is represented by multiple overlapping concordant grains with small analytical uncertainties and the age distribution shows a clear youngest peak separated from older populations. In contrast, where the youngest grains are scarce, dispersed in age, or associated with large analytical uncertainties, the calculated MDA is interpreted strictly as a maximum constraint on deposition and may significantly predate sediment accumulation. Samples yielding < 10% concordant grains or large MLA uncertainties (>±10–15 Ma) are regarded as weakly constrained.

4. Results

4.1. U-Pb dating of detrital zircons from Dajarra region

All samples were collected from the Dajarra region with the aim of constraining the maximum depositional ages (MDAs) of metasedimentary units, which are generally interpreted as a continuation of the stratigraphic sequences exposed in the northern part of the WS. The MDA results are summarised in Table 1, and the U-Pb data are provided in Supplementary Material A.

The robustness of MDAs varies between samples depending on the number of concordant grains and the coherence of the youngest age population. Samples with large numbers of concordant grains forming a well-defined youngest cluster (e.g., SP18, SP25, SP45 and SP50) provide relatively strong depositional constraints. In contrast, samples yielding few concordant grains (e.g., SP03 and SP28) or dispersed youngest ages produce weaker MDAs that should be regarded primarily as maximum age constraints rather than precise depositional ages.

4.1.1. Mount Guide Quartzite

In the Dajarra region, the units mapped as the Mount Guide Quartzite form a NNE-trending belt of prominent ridges and hills in the eastern part of the Leichhardt River domain, along the contact with the Kalkadoon-Leichhardt domain (Fig. 3). The unit is predominantly composed of quartzite, feldspathic meta-arenite, and sericitic meta-arenite. It overlies metagreywacke, conglomerate, and minor quartzite of the Yappo Member, which is regarded as the lower part of the Mount Guide Quartzite. The unit is mapped in conformable contact with the underlying Bottletree Formation and is overlain by the Eastern Creek Volcanics. The unit is complexly folded and crosscut by a series of northwest trending faults with apparent sinistral displacement (Fig. 4a). Along the eastern margin, near the contact with the Bottletree Formation, the bedding is locally overturned. It is intruded by north–south trending, undeformed and coarse-grained porphyry dykes collectively mapped as the Garden Creek Porphyry. Two quartzite samples were collected from the Mount Guide Quartzite from different outcrops.

4.1.1.1. Sample SP18. Sample SP18 was collected from a bedded quartzite, located ~ 7 km NE of Dajarra town (Fig. 4a) near the contact with the Yappo Member and the Bottletree Formation, thus most likely representing the lowermost part of the unit. The bedding at this location dips ~ 50° towards WNW whereas near the contact with the Yappo Member the bedding is overturned and dips ~ 70° ESE indicating complex internal folding. The sample is a coarse grained, white to pale-greyish feldspathic quartzite (Fig. 5a). Zircons grains separated from this sample are uniform in size, ranging from 62 to 124 μm in length and are colourless and transparent. They have euhedral to anhedral shapes with minor fracturing and few mineral inclusions. Cathodoluminescence imaging reveals internal features that range from well-defined oscillatory zoning to featureless dark zones (Fig. 6a).

A total of 235 grains were analysed from sample SP18, of which 188 analyses were discordant and excluded from further consideration. The remaining 39 zircon grains yield ages ranging from ca. 2610 Ma to 1836 Ma. Of these, 33 grains are younger than 2100 Ma and form a dominant age cluster (Fig. 7a) with a $^{207}Pb/^{206}$-Pb weighted average age of 1882 ± 6 Ma (MSWD = 1.50) defined by the youngest 28 analyses. This result is consistent with the minimum $^{207}Pb/^{206}Pb$ age of 1883 ± 7 Ma obtained using the MLA method. Accordingly, the age of 1883 ± 7 Ma is interpreted as the maximum depositional age (MDA) for this feldspathic quartzite.

4.1.1.2. Sample SP26. Sample SP26 was collected approximately 5 km west of Dajarra township (Fig. 4a) near the contact with the ECVs thus most likely representing the upper part of the unit. The quartzite is thickly bedded at this location, trends NW and dips moderately to shallow towards SE (Fig. 4a). The collected sample is a greyish, feldspathic to micaceous coarse-grained quartzite (Fig. 5b). Zircon grains are variable in size, range between 45 and 145 μm in length and exhibit euhedral to subhedral shapes. Their colour varies between yellowish to brownish to colourless whereas fracturing and mineral inclusions are common. All grains display oscillatory zoning and have low luminescence (Fig. 6b).

Table 1
Summary of $^{207}Pb/^{206}Pb$ ages and the interpreted MDAs for metasedimentary rocks in the Dajarra region. Coordinates are GDA94 UTM.

Stratigraphic unit	Sample	Easting	Northing	Weighted average age (Ma)	MLA age (Ma)	Age comment
Mount Guide Quartzite	**SP18**	350,716	7,606,734	1882 ± 6[1]	**1883 ± 7[2]**	[1]n = 28; MSWD = 1.5; [2]n = 39
	SP26	341,431	7,599,789	1851 ± 4[1]	**1842 ± 9[2]**	[1]n = 19; MSWD = 1.5; [2]n = 102
Eastern Creek Volcanics	**SP34**	343,241	7,600,077	1876 ± 6[1]	**1877 ± 8[2]**	[1]n = 18; MSWD = 1.5; [2]n = 42
	SP35	339,188	7,600,963	1778 ± 9[1]	**1766 ± 15[2]**	[1]n = 8; MSWD = 0.7; [2]n = 114
Jayah Creek Metabasalt	**SP37**	337,183	7,600,039	1865 ± 3[1]	**1857 ± 5[2]**	[1]n = 47; MSWD = 1.2; [2]n = 162
Timothy Creek Sandstone	**SP03**	335,589	7,599,844	1783 ± 12[1]	**1781 ± 15[2]**	[1]n = 10; MSWD = 0.8; [2]n = 27
Warrina Park Quartzite	**SP25**	338,739	7,600,642	1812 ± 4[1]	**1812 ± 5[2]**	[1]n = 39; MSWD = 1.4; [2]n = 75
	SP28	349,781	7,569,577	1863 ± 8[1]	**1862 ± 9[2]**	[1]n = 11; MSWD = 1.6; [2]n = 20
	SP30	349,999	7,569,577	1788 ± 4[1]	**1781 ± 10[2]**	[1]n = 27; MSWD = 1.3; [2]n = 63
Moondarra Siltstone	**SP45**	338,586	7,600,616	1776 ± 5[1]	**1776 ± 6[2]**	[1]n = 47; MSWD = 1.3; [2]n = 64
Kallala Quartzite	**SP48**	316,981	7,567,294	1825 ± 3[1]	**1812 ± 8[2]**	[1]n = 58; MSWD = 1.3; [2]n = 129
	SP50	317,359	7,566,391	1851 ± 3[1]	**1850 ± 4[2]**	[1]n = 93; MSWD = 1.2; [2]n = 150

Fig. 5. Field photographs of representative outcrops of metasedimentary rocks in the Dajarra region. (a) Quartzite (SP18) mapped as Mount Guide Quartzite intruded by the Garden Creek Porphyry; (b) Mount Guide Quartzite exposed along a road cut (SP26); (c) massive bedded-quartzite unit on the eastern side of the Eastern Creek Volcanics (SP34); (d) conglomeratic greywacke along the western part of the Eastern Creek Volcanics (SP35); (e) quartzite outcrop along a road cut, representing intercalated sedimentary rocks part of the Jayah Creek Metabasalt (SP37); (f) bedded meta-arenite mapped as Timothy Creek Sandstone (SP03); (g) roadcut outcrop of quartzite mapped as Warrina Park Quartzite (SP25); (h) metasiltstone of Moondarra Siltstone (SP45); (i) exposure of quartzite (SP48) and (j) feldspathic quartzite (SP50) forming the Kallala Quartzite. Foliated exposure of (k) quartzite (SP28) and (l) volcanoclastic rock (SP30) mapped as Warrina Park Quartzite from the southern part of Dajarra region.

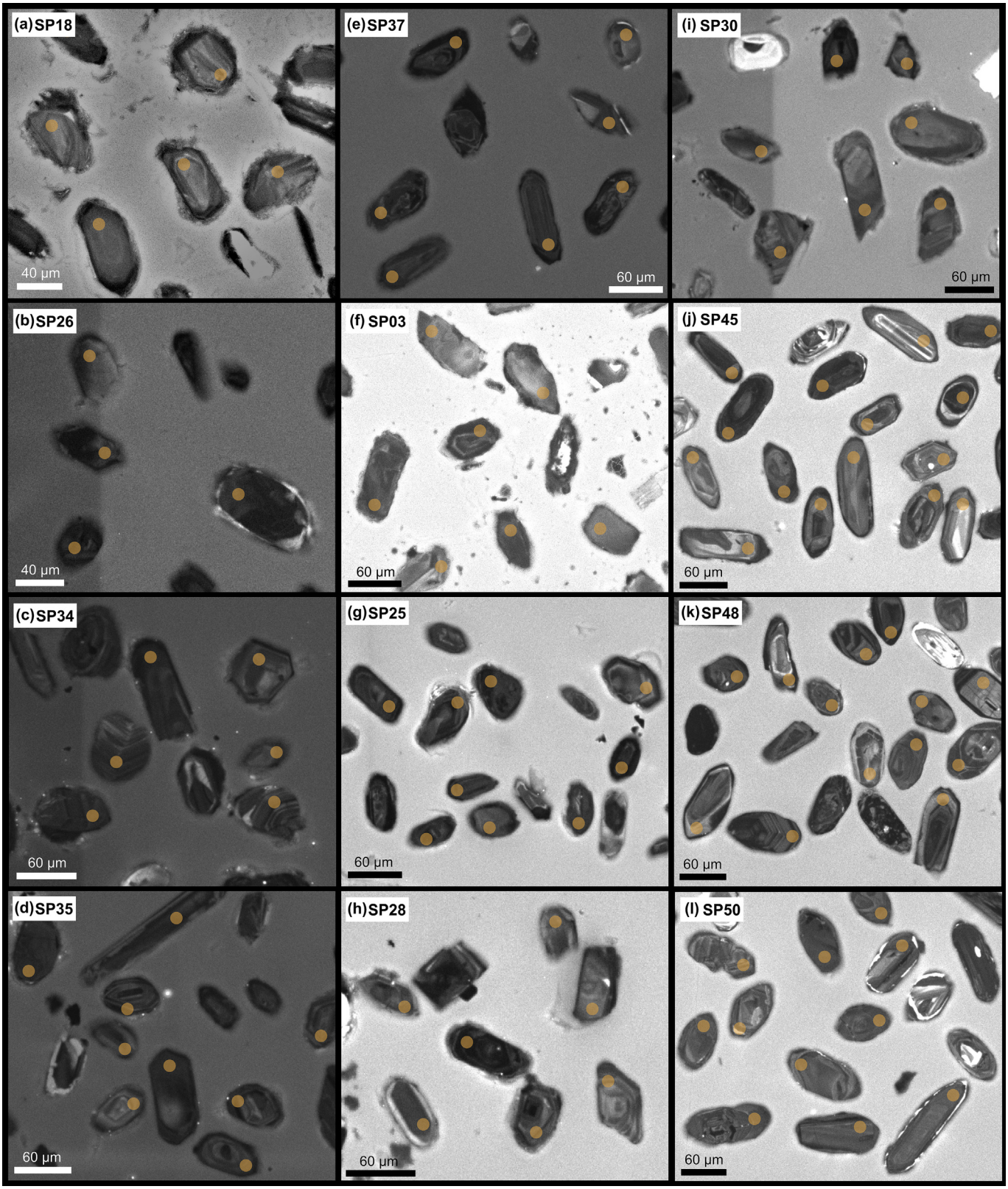

Fig. 6. Cathodoluminescence (CL) images of detrital zircon grains from samples in the Dajarra region, showing internal structures and locations of U-Pb analytical spots.

A total of 277 grains were analysed from this sample of which 175 grains were discordant and eliminated from further consideration. The remaining 102 grains yielded ages between ca. 2900 Ma and 1823 Ma. Of these, 73 grains fall within the range of 2100–1823 Ma and define prominent peaks at 2047 Ma, 1993 Ma and 1940 Ma (Fig. 7b). The youngest population, represented by 28 grains, yields a $^{207}Pb/^{206}Pb$ weighted average age of 1851 ± 4 Ma (MSWD = 1.50) based on the 19 youngest concordant grains. To

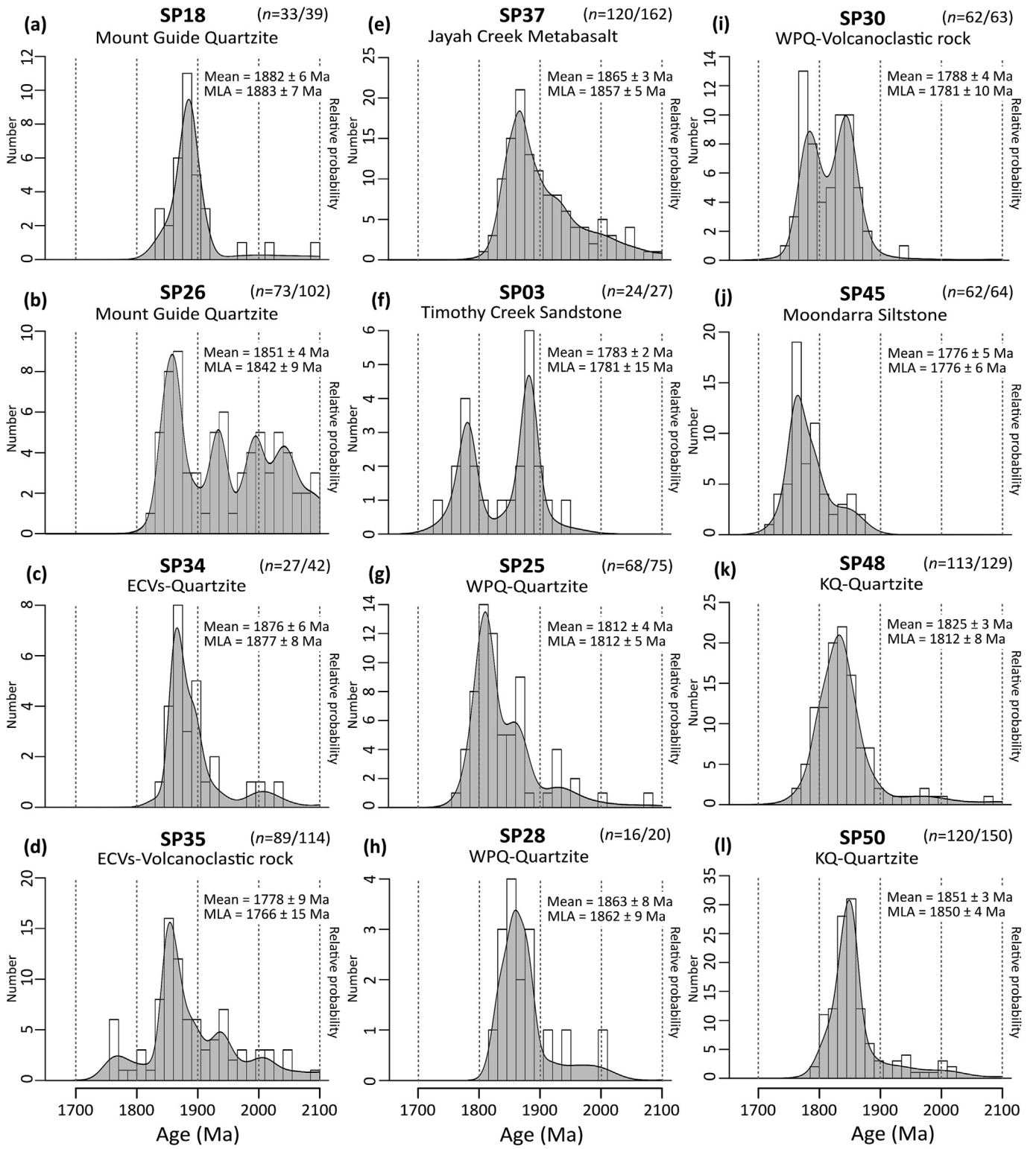

Fig. 7. Probability density diagrams and histograms of detrital zircon age distributions from metasedimentary rocks in the Dajarra region. The data represent $^{207}Pb/^{206}Pb$ ages and are within the age range of 2100 Ma to 1650 Ma. Analyses exhibiting more than 10% discordance have been excluded. Full name of abbreviations: ECVs = Eastern Creek Volcanics, WPQ = Warrina Park Quartzite, KQ = Kallala Quartzite.

mitigate potential bias, the MLA estimation was also applied, yielding a minimum $^{207}Pb/^{206}Pb$ age at 1842 ± 9 Ma which is similar within error to the $^{207}Pb/^{206}Pb$ weighted average age and is considered the maximum depositional age (MDA) for sample SP26.

4.1.2. Eastern Creek Volcanics

The Eastern Creek Volcanics (ECVs) in the Dajarra region form an NNW-trending belt, predominantly occurring east of the Wonomo Fault within the Leichhardt River domain (Fig. 3). The

unit is characterized by massive metabasalt interlayered with metasedimentary rocks, including quartzite, meta-arenite, conglomeratic metagreywacke, and feldspathic metasandstone. It is interpreted to be underlain by the Mount Guide Quartzite. The contact with Warrina Park Quartzite is not exposed but it is assumed to be unconformable. Two samples were collected from the Eastern Creek Volcanics to represent different rock units and the western and eastern area of exposure (Fig. 4a).

4.1.2.1. Sample SP34. Sample SP34 was collected from the eastern part of the ECVs (Fig. 4a), where the unit is exposed as north–south trending ridge. The clastic unit is dominated by red-brown feldspathic quartzite intercalated with quartz sandstone, minor conglomerate and pebbly sandstone. The quartzite (Fig. 5c) has well-preserved graded bedding, is steeply dipping and shows evidence of small-scale folding, but no large-scale folds were recognised. The quartzite unit is ~ 9 km long, up to 400 m wide and is bounded on both sides by ECVs mafic rocks although no contact was observed in this study. The sedimentary unit at this location is foliated although the intensity of foliation is variable. Zircon grains separated from this sample are rounded and the length ranges from 60–130 μm. Their colour varies from brownish to yellowish to colourless and commonly are fractured and contain mineral inclusions. The CL images reveal oscillatory zoning, core-rim structures and homogeneous textures with moderate to low luminescence (Fig. 6c).

Of the 210 zircon grains analysed from sample SP34, only 41 grains fall within the ± 10% discordance threshold and were used for MDA interpretation. These concordant grains yield ages ranging from ca. 2847 Ma to 1836 Ma. Among them, 26 grains with ages younger than 2100 Ma define two distinct age clusters: one between ca. 2031–1994 Ma and another between ca. 1932–1836 Ma (Fig. 7c). The latter yields a $^{207}Pb/^{206}Pb$ weighted average age of 1876 ± 6 Ma (n = 18, MSWD = 1.50). This result is consistent with the $^{207}Pb/^{206}Pb$ age of 1877 ± 8 Ma obtained using the MLA approach. Consequently, the age of 1877 ± 8 Ma is interpreted to represent the maximum depositional age (MDA) of this quartzite.

4.1.2.2. Sample SP35. Sample SP35 was collected from the western part of the ECVs near the contact with the Warrina Park Quartzite from an outcrop of conglomeratic metagreywacke (Fig. 4a and Fig. 5d). The conglomeratic metagreywacke outcrop forms a small hill and is ~ 1 km long and up to 150 m wide unit. The surrounding mafic rocks of the ECVs consist of massive basalts that is fine grained, not foliated, and preserves vesicular textures. In addition, flow-top breccias are well preserved approximately 500 m north of the sampling location. Locally, within the mafic units, few meters wide zones of foliated rocks can be found and could represent localised shear zones since most of the mafic units lack a deformation fabric at this location. The selected sample is a dark grey, medium-grained metagreywacke. Similar looking metagreywacke units occur along the road cut to Dajarra town where they appear to be in transitional contact with the overlying Warrina Park Quartzite. The selected sample contains subrounded zircon grains ranging from 60 to 180 μm and exhibiting a colour range from yellowish to colourless. The zircon grains are commonly fractured and contain mineral inclusions. The cathodoluminescence images show oscillatory zoning patterns and a few grains display core-rim structures (Fig. 6d).

A total of 263 zircon grains were analysed from sample SP35. Of these, 149 grains were excluded from further interpretation due to high degrees of discordance. The 114 remaining grains yield ages ranging from ca. 2794 Ma to 1757 Ma. Three minor age clusters are identified from 25 grains, with peaks at ca. 2529 Ma, ca. 2434 Ma, and ca. 2146 Ma. The remaining 89 grains show subordinate peaks at ca. 2012 Ma and ca. 1942 Ma, and a dominant population peak at approximately 1860 Ma (Fig. 7d). The youngest zircon population yields a $^{207}Pb/^{206}Pb$ weighted average age of 1778 ± 9 Ma (MSWD = 0.70) calculated from the eight youngest concordant grains. All concordant grains from this sample produced an MLA age of 1766 ± 15 Ma, which is interpreted as the maximum depositional age for the conglomeratic metagreywacke.

4.1.3. Jayah Creek Metabasalt

The Jayah Creek Metabasalt forms an NNW-trending belt, predominantly occurring west of the Wonomo Fault within the Leichhardt River domain (Fig. 3). It is composed mainly of amphibolitic metabasalts intercalated with metasedimentary rocks, including quartzite and micaceous to feldspathic *meta*-arenite. In the western part, the Jayah Creek Metabasalt is in structural contact with Alpha Centauri Metamorphics and the Steeles Granite whereas in the eastern part it is in structural contact with the Moondarra Siltstone.

Sample SP37 was collected from a quartzite belonging to a metasedimentary unit intercalated with the Jayah Creek Metabasalt and cropping out along a roadcut exposure on the Boulia-Mount Isa Highway (Fig. 4a). The unit is 200 m wide, trends ~ 7 km north–south and is displaced dextrally by NE and NW trending faults. At the sampling location the metasediments are strongly deformed, trend north south and dip steeply west (Fig. 5e). Zircon grains extracted from sample SP37 are euhedral to subhedral with moderately rounded edges and are predominantly colourless. Their sizes range from 50 to 110 μm. The cathodoluminescence images reveal variable internal structures, including oscillatory zoning and recrystallization textures (Fig. 6e).

A total of 270 zircon grains were analysed, of which 108 grains have high levels of discordance and were excluded from further interpretation. The remaining 162 grains have U-Pb ages between ca. 2734 Ma and 1812 Ma. The oldest population is identified at ca. 2697 Ma and followed by a population cluster ranging from ca. 2600 Ma to 2500 Ma. The predominant age population occurs between 2000 Ma and 1812 Ma and contains the youngest population of this sample (Fig. 7e). The $^{207}Pb/^{206}Pb$ weighted average age of the youngest group is 1865 ± 3 Ma (n = 47, MSWD = 1.20). The minimum age of this sample using the MLA method is 1857 ± 5 Ma. The MLA age is interpreted as the maximum depositional age for this quartzite unit within the Jayah Creek Metabasalt.

4.1.4. Timothy Creek Sandstone

The Timothy Creek Sandstone refers to a massive sequence of sericitic *meta*-arenite exposed approximately 12 km west of Dajarra town, forming a NNW-trending belt of prominent ridges and hills within the Leichhardt River domain (Fig. 3). This unit preserves primary sedimentary structures including crossbedding and ripple marks. It has been interpreted as interlayered metasedimentary rocks within the Jayah Creek Metabasalt.

Sample SP03 was collected from a NNW–SSE trending bedded sericite quartzite unit dipping moderately to the west (Fig. 4a and Fig. 5f). At the location of the sampling area, cross bedding indicates younging towards the west. Zircon grains extracted from sample SP03 are rounded, and range in length from 40 to 120 μm. The zircon grains vary in colour from yellowish to colourless and often contain mineral inclusions. The cathodoluminescence imaging reveals oscillatory zoning with generally low CL emission (Fig. 6f).

A total of 252 grains were analysed, of which only 27 grains had less than 10% discordance and were used for further consideration. These grains yielded ages from ca. 2591 Ma to 1740 Ma. Three zircon grains define a population cluster with a peak at ca. 2579 Ma. The remaining grains reveal a bimodal age distribution, with clusters between ca. 1930–1845 Ma and ca. 1815–1745 Ma (Fig. 7f). The youngest population cluster yields a $^{207}Pb/^{206}Pb$ weighted

average age of 1783 ± 12 Ma (n = 10, MSWD = 0.80). This result is consistent with a minimum $^{207}Pb/^{206}Pb$ age of 1781 ± 15 Ma obtained by using the MLA method which is considered the maximum depositional age for this sample.

4.1.5. Warrina Park Quartzite

The Warrina Park Quartzite forms as a NNW-trending belt which is predominantly exposed adjacent to the Wonomo Fault (Fig. 3). It is characterized by *meta*-arenite and quartzite with minor occurrences of conglomerate and metasiltstone and is assigned to the basal formation of the Mount Isa Group. In the northern part, this unit occurs in proximity to the ECVs (sample SP25; Fig. 4a). In the southeastern part of the Leichhardt River domain, near the contact with the Kalkadoon-Leichhardt domain, a series of rocks units are mapped as belonging to the Warrina Park Quartzite (Blake et al., 1982), but their exact stratigraphic position and relationship with the surrounding rocks is poorly constrained due to limited outcrop exposure. Two samples (SP28 and SP30; Fig. 4c) were collected from this part of the region to check if they display detrital zircon patterns similar to the units mapped as Warrina Park Quartzite. The outcrop in the region consists of low-lying rock intermittently exposed along and across strike. Most of the area is covered by thin clay, silt, gravel and soil. No contacts with adjacent units have been observed.

4.1.5.1. Sample SP25. Sample SP25 was sampled from a roadcut exposure of quartzite along the Boulia-Mount Isa Highway, approximately 8 km west of Dajarra. At this location, the Warrina Park Quartzite is thin to thickly bedded, trends NNW-SSE and dips steeply west (Fig. 5g). Sample SP25 is a pale grey, coarse grained feldspathic quartzite. Zircon grains are uniformly euhedral with moderately rounded edges, range in colour from yellowish to colourless, and measure between 50 and 200 μm in length. The internal structure of zircon grains is dominated by oscillatory zoning and distinct growth zones with moderate CL emission (Fig. 6g).

A total of 303 zircon grains were analysed from sample SP25 and only 75 grains were less than 10% discordant and used for further interpretation. A small number of grains yielded ages older than 2100 Ma, forming a minor peak at ca. 2330 Ma. The remaining analyses define a minor peak at around 1931 Ma and a dominant population ranging from ca. 1890 Ma to 1770 Ma (Fig. 7g). Within this range, a minor population is identified at ca. 1862 Ma, whereas the major population consisting of the youngest grains yields a $^{207}Pb/^{206}Pb$ weighted average age of 1812 ± 4 Ma (n = 39, MSWD = 1.40). This result is consistent with the MLA age of 1812 ± 5 Ma. Accordingly, the age of 1812 ± 5 Ma is interpreted as the maximum depositional age for the Warrina Park Quartzite at this location.

4.1.5.2. Sample SP28. This sample was collected from an intensely deformed feldspathic quartzite, trending NNW–SSE and steeply to moderately towards the east (Fig. 5k). Zircon grains separated from this sample, range in size from 50 to 190 μm, are moderately to highly rounded and predominantly yellowish to colourless. Cathodoluminescence (CL) imaging reveals oscillatory growth zoning, characterized by low CL emission and distinct core-rim structures (Fig. 6h).

A total of 256 zircon grains were analysed from sample SP28 with 236 analyses showing a high degree of discordance and removed from further interpretation. The remaining 20 concordant grains have U-Pb ages ranging from ca. 2640 Ma to 1830 Ma. The dominant detrital zircon population is defined between ca. 1890 Ma and 1830 Ma (Fig. 7h). The $^{207}Pb/^{206}Pb$ weighted average age obtained from the youngest population is 1863 ± 8 Ma (n = 11, MSWD = 1.60). The MLA age of this sample is 1862 ± 9 Ma and is considered the maximum depositional age for this unit at this location.

4.1.5.3. Sample SP30. Sample SP30 was collected from a deformed volcaniclastic horizon trending NNW-SSE and dipping steeply east (Fig. 4c). On the geological maps the location of this sample is mapped as Warrina Park Quartzite. The volcanoclastic unit occurs as discontinuous lens-shaped bodies that that form small outcrops and define the regional structural trend (Fig. 5l). No contact with the feldspathic quartzite or other rocks has been identified in the field. Zircon grains separated from this sample range in length from 60 to 150 μm and exhibit euhedral to anhedral morphologies with moderate degrees of roundness. The grains are pale yellow to colourless and commonly display minor fracturing and the presence of mineral inclusions. The CL images reveal oscillatory growth zoning, characterized by moderate to low CL emission and well-defined core-rim structures (Fig. 6i).

A total of 194 grains were analysed from sample SP30, of which 131 grains are classified as discordant data and removed from interpretation. The 63 concordant grains display a bimodal age distribution, with two distinct clusters spanning between ca. 1890–1820 Ma and ca. 1815–1770 Ma (Fig. 7i). The older population yields a $^{207}Pb/^{206}Pb$ weighted average age of 1847 ± 4 Ma (n = 27, MSWD = 1.30), whereas the youngest population yields a $^{207}Pb/^{206}Pb$ weighted average age of 1788 ± 4 Ma (n = 27, MSWD = 1.30). The minimum age determined by the MLA method, is 1781 ± 10 Ma and is interpreted as the maximum depositional age of the volcaniclastic rock unit.

4.1.6. Moondarra Siltstone

The Moondarra Siltstone is composed predominantly of pyritic metasiltstone with minor carbonaceous shale and limestone. The unit is sheared, shows complex internal folding and contains numerous quartz veins. It trends NNW-SSE and dips steeply west. The contact with the Warrina Park Quartzite and the Jayah Creek Metabasalt is not exposed but at this location the contact with the Jayah Creek Metabasalt is likely structural controlled. The metamorphic grade is lower to middle greenschist facies. Sample SP45 was collected from a dolomitic siltstone, containing minor pyrite and crosscut by quartz veins (Fig. 5h).

Zircon grains extracted from sample SP45 are predominantly euhedral with moderate roundness, ranging in length from 50 to 160 μm. The grains vary in colour from yellowish to colourless and commonly exhibit minor fractures and mineral inclusions. The CL images expose internal features such as oscillatory zoning and core-rim structures (Fig. 6j).

A total of 309 zircon grains were analysed, of which 245 analyses showed a high degree of discordance and were excluded from interpretation. The remaining 64 concordant grains include two grains dated at approximately 2500 Ma, whereas 62 grains define a broad age distribution ranging from ca. 1890 Ma to 1725 Ma (Fig. 7j). Within this broad distribution, a minor cluster is identified at ca. 1858 Ma. The main cluster contains the youngest population with a $^{207}Pb/^{206}Pb$ weighted average age of 1776 ± 5 Ma (n = 47, MSWD = 1.30) which is identical to the MLA age of 1776 ± 6 Ma considered the maximum depositional age of the Moondarra Siltstone at this location.

4.1.7. Kallala Quartzite

The Kallala Quartzite forms an ~ 10 km long and 2 km wide, north-trending unit in the southern part of the Sybella domain (Fig. 3). It forms high ridges composed of quartzite and feldspathic quartzite, with minor schist and gneiss. On the eastern side the unit is in contact with the Sulieman Gneiss whereas on the southern and western part it is in contact with the Alpha Centauri Metamorphics. To the north the Kallala Quartzite is in contact with and

intruded by granite mapped as part of the Sybella Igneous Event. The contact with the Sulieman Gneiss was assumed to be gradational and thus is interpreted to be part of the Pre-Barramundi basement (Blake et al., 1984). Two samples were collected from different topographic levels within this unit: sample SP48 was collected from a high ridge, whereas sample SP50 was obtained from an outcrop along a valley (Fig. 4b).

4.1.7.1. Sample SP48. Sample SP48 was collected from an outcrop of white, coarse-grained quartzite located along a ridge within this unit (Fig. 5i). Zircon grains extracted from sample SP48 are predominantly euhedral to moderately rounded, colourless, and have lengths ranging from 40 to 180 μm. Most zircon grains exhibit variable internal structures, including oscillatory zoning, core-rim structures and evidence of recrystallization (Fig. 6k).

A total of 295 grains were analysed from this sample with 166 grains having more than 10% discordance and excluded from further analyses. The remaining 129 grains yield ages spanning from ca. 2790 Ma to 1755 Ma. Within this range, two population clusters are delineated: a minor, older population between ca. 2520 Ma and 2415 Ma, and a predominant younger population between ca. 1905 Ma and 1755 Ma (Fig. 7k). The youngest population yields a ^{207}Pb/^{206}Pb weighted average age of 1825 ± 3 Ma (n = 58, MSWD = 1.30) whereas the MLA method yields a minimum age of 1812 ± 8 Ma which is interpreted to represent the maximum depositional age for the sample SP48.

4.1.7.2. Sample SP50. Sample SP50 is a feldspathic quartzite collected from a creek bed (Fig. 5j). Zircon grains extracted from this sample are characterized by euhedral to subhedral grains with rounded edges, ranging in length from 60 to 200 μm. The zircon grains vary in colour from yellowish to colourless and commonly contain mineral inclusions. Cathodoluminescence images reveal internal structures including oscillatory zoning and core–rim features (Fig. 6l).

A total of 199 grains were analysed with 49 grains excluded from further analyses due to high discordance. The remaining 150 grains have U-Pb ages between ca. 2757 Ma and 1789 Ma. The age distribution reveals a minor cluster peaking at ca. 2512 Ma and a dominant population between ca. 2040 Ma and 1785 Ma (Fig. 7l). Within this major age range, a ^{207}Pb/^{206}Pb weighted average age of 1851 ± 3 Ma (n = 93, MSWD = 1.20) is obtained from the youngest population. The MLA analysis yields a similar age of 1850 ± 4 Ma which interpreted as the maximum depositional age of the feldspathic quartzite.

4.2. Zircon Hf isotope compositions

Hafnium isotopic analyses were conducted on 99 zircon grains from eleven metasedimentary samples representing new maximum depositional ages from the Dajarra region. The results are shown as $\varepsilon_{Hf}(t)$ values plotted against the interpreted crystallization ages (Fig. 8). The $\varepsilon_{Hf}(t)$ values were calculated using the individual crystallization age of each detrital zircon grain.

Detrital zircons from the Mount Guide Quartzite (SP18 and SP26) yield $\varepsilon_{Hf}(t)$ values that cluster around the CHUR line. In both samples, zircons dated between ca. 1900 Ma and 1840 Ma record $\varepsilon_{Hf}(t)$ values ranging from –4.7 to +2.2, whereas late Archean to early Paleoproterozoic grains (ca. 2600–2400 Ma) show values between –1.7 and +3.3.

In the Eastern Creek Volcanics, the quartzite (SP34) and conglomeratic greywacke (SP35) yield broadly similar patterns. The youngest single zircon at ca. 1758 Ma records an $\varepsilon_{Hf}(t)$ value of –5.2. Detrital zircons dated between ca. 2100 Ma and 1840 Ma display values ranging from –5.2 to +5.5, although strongly unradiogenic grains are also present (–13.1 and –10.5). Older detrital grains between ca. 2550 Ma and 2300 Ma yield $\varepsilon_{Hf}(t)$ values between –5.1 and +2.1.

The feldspathic quartzite from the Jayah Creek Metabasalt (SP37) has a major zircon age cluster between ca. 2100 Ma and 1840 Ma, with $\varepsilon_{Hf}(t)$ values from –3.4 to +1.2, along with a single strongly unradiogenic grain at –10.5.

The Timothy Creek Sandstone (SP03) shows a distinct bimodal age distribution. The younger cluster records $\varepsilon_{Hf}(t)$ values close to CHUR, between –3.4 and +0.3, whereas the older cluster is more unradiogenic, ranging from –5.6 to –1.0. A single zircon dated at ca. 2500 Ma records $\varepsilon_{Hf}(t)$ of –0.2.

The Warrina Park Quartzite (SP25) preserves more radiogenic Hf signatures overall. Zircons dated between ca. 1820 Ma and 1780 Ma record $\varepsilon_{Hf}(t)$ values between +0.6 and +8.7, while a grain at ca. 1850 Ma yields +0.2. In contrast, the Moondarra Siltstone (SP45) shows a wider range of compositions, with zircons between ca. 1800 Ma and 1740 Ma recording $\varepsilon_{Hf}(t)$ values from –6.7 to +3.5, and a ca. 1850 Ma grain aligned with CHUR. Limited zircon data were obtained from samples SP28 and SP30. From the quartzite sample (SP28) only one grain was analysed with a ^{207}Pb/^{206}Pb age of ca. 1860 Ma and yielded a $\varepsilon_{Hf}(t)$ of +0.9. The volcaniclastic sample (SP30) shows a bimodal distribution comparable to the Timothy Creek Sandstone, with the youngest subpopulation (ca. 1790–1780 Ma) yielding $\varepsilon_{Hf}(t)$ values between –2.7 and +0.4, and the older subpopulation (ca. 1850–1840 Ma) has $\varepsilon_{Hf}(t)$ values ranging from –3.0 to +3.9.

The Kallala Quartzite (SP48) is characterized by zircons dated between ca. 1850 Ma and 1820 Ma, which yield $\varepsilon_{Hf}(t)$ values between –2.3 and +1.1. An older ca. 2400 Ma grain records a more radiogenic value of +3.1.

5. Discussion

5.1. Timing of deposition and stratigraphic correlations

The sedimentary units from the Dajarra region are part of the Leichhardt River domain and were attributed to the Leichhardt and Calvert Superbasins sequences (e.g. Gibson et al., 2016). Recent work has shown that the Leichhardt Superbasin sequences extend further south under the Georgina Basin until the Cork Fault (e.g. Spampinato et al., 2015; Olierook et al., 2022). Our results indicate that the MDAs for most sedimentary sequences (the Mount Guide Quartzite, ECVs, Jayah Creek Metabasalt, Warrina Park Quartzite, Moondarra Siltstone and Kallala Quartzite) in the Dajarra region are very different from the MDAs of stratigraphic equivalents in the northern part of the inlier suggesting either different sources or that the stratigraphy is not as continuous as previously believed (Fig. 9).

The Mount Guide Quartzite was mapped as a relatively continuous unit from the northern part of the inlier to the Dajarra region and extending undercover until the Cork Fault (e.g. Spampinato et al., 2015). Our results indicate MDAs of 1883 ± 7 Ma for sample SP18 and 1842 ± 9 Ma for sample SP26 which are significantly older compared to MDAs reported from the northern part of the inlier. Neumann et al. (2006) reported MDAs of 1793 ± 9 Ma for the lower Mount Guide Quartzite and 1773 ± 16 Ma for the upper Mount Guide Quartzite from samples collected east of Mount Isa town. They interpreted the minimum age for the sequence to be ca. 1785 Ma. The MDA discrepancy cannot be explained by a lack of 1790 Ma to 1770 Ma igneous rocks in the Dajarra region since igneous rocks within this age range were reported from the Tick Hill and Dajarra regions (e.g. Le et al., 2021b; Cocker et al., 2025; Noptalung et al., 2026). Moreover, the units mapped as Mount Guide Quartzite in the Dajarra region are intruded by the Garden Creek Porphyry dated at 1783 ± 5 Ma (Noptalung et al., 2026).

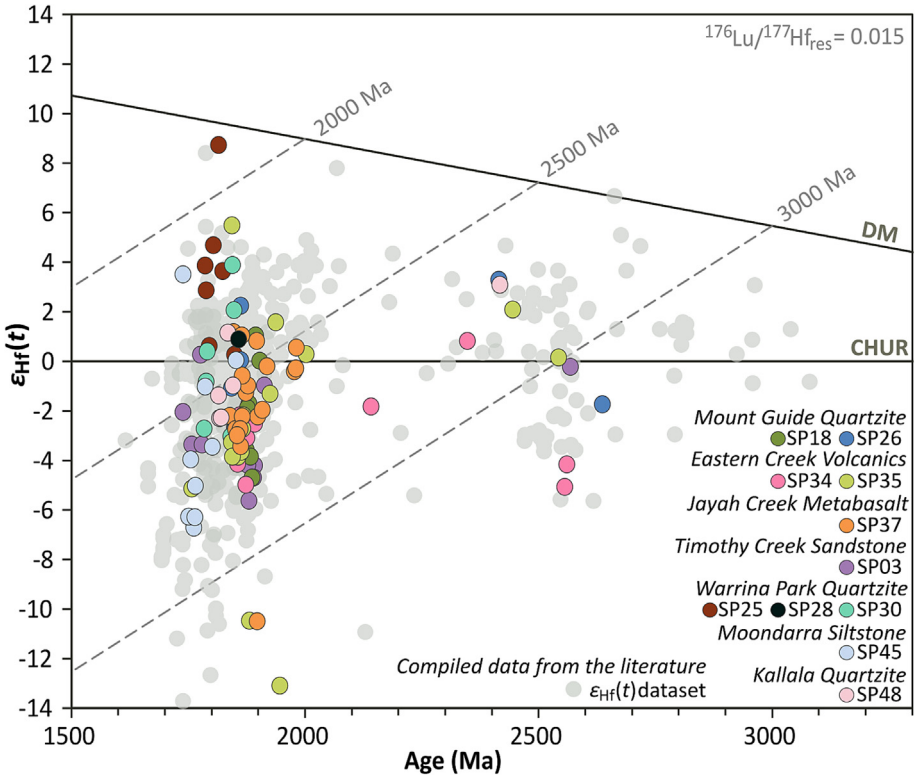

Fig. 8. Hf isotopic data of detrital zircons from metasedimentary rocks in the Dajarra region with the $\varepsilon_{Hf}(t)$ dataset from previous studies (Bierlein et al., 2011; Lewis et al., 2022; Olierook et al., 2022; Noptalung et al., 2026). $^{176}Lu/^{177}Hf_{res}$ = 0.015 (ε_{Hf}/Ma = 0.012; slope of evolution lines), regarding to evolution lines of Proterozoic shales (Vervoort and Blichert-Toft, 1999; Spencer et al., 2020). Full name of abbreviations: CHUR = chondritic uniform reservoir, DM = depleted mantle.

The Garden Creek Porphyry is undeformed and intrudes the folded quartzite suggesting that the rocks mapped as Mount Guide Quartzite in the Dajarra region are older and are not stratigraphically equivalent to the units mapped in the northern part of the inlier.

Comparable to the Mount Guide Quartzite, the ECVs were mapped as a relatively continuous stratigraphic unit from the northern part of the inlier to the Dajarra region and further undercover until the Cork Fault (e.g. Spampinato et al., 2015). Our results show two significantly different MDAs from metasedimentary units intercalated with the mafic volcanics. The quartzite sample (SP34) from the western part has an MDA of 1877 ± 8 Ma, whereas the conglomeratic greywacke sample (SP35) from the eastern part has and MDA of 1766 ± 15 Ma (Fig. 7c and d; Table 1). The detrital zircon age distribution for the quartzite sample SP34 closely resembles that of sample SP18 collected from the eastern Mount Guide Quartzite (Fig. 10), particularly in the dominance of Paleoproterozoic age populations between ca. 1900–1800 Ma. Although the number of concordant analyses in SP34 is moderate, the similarity in principal age modes, combined with the presence of a well-developed ductile fabric comparable to that observed in the Mount Guide Quartzite, suggests that the quartzite unit mapped as part of the ECVs (SP34) may instead belong to the Mount Guide Quartzite. We therefore interpret this reassignment as plausible but acknowledge that it is based on integrated provenance and structural evidence rather than zircon age data alone. The conglomeratic greywacke (SP35) does not have a ductile fabric, is steeply dipping and younging towards the west. This is consistent with the steeply dipping and younging west observations across the ECVs, as indicated by individual layers containing vesicles and flow top breccia, and the lack of a ductile fabric. Based on depositional age similarities between the ECVs and the Myally Subgroup, Neumann et al. (2006) proposed that the ECVs could be included with the Myally Subgroup rather than the Mount Guide Quartzite. They proposed that the deposition of the Myally Subgroup ceased at ca. 1765 Ma. This age is consistent with the MDA of 1766 ± 15 Ma obtained from the conglomeratic metagreywacke (SP35) indicating that indeed the ECVs extend into the Dajarra region and probably further south undercover.

The Jayah Creek Metabasalt was interpreted to be equivalent with the ECVs, whereas the Timothy Creek Sandstone was interpreted to be equivalent with the Lena Quartzite (Derrick et al., 1976) and occur as a conformable layer within the Jayah Creek Metabasalt (Blake et al., 1984). Our observations suggest that the Timothy Creek Sandstone unconformably overlies the Jayah Creek Metabasalt, although the nature of this unconformity is unclear. The layering in the Timothy Creek Sandstone dips moderately (~40°–50°) west, whereas the units forming the Jayah Creek Metabasalt are sub-vertical consistent with an angular unconformity between these two units. Whereas the MDA obtained from a quartzite layer within the Jayah Creek Metabasalt is 1857 ± 5 Ma, the MDA obtained from the Timothy Creek Sandstone is 1781 ± 15 Ma. The mafic units of the Jayah Creek Metabasalt and the intercalated metasediments contain a well-defined schistosity and are metamorphosed to lower amphibolite facies. This is very different to the ECVs in the east which lack ductile deformation, and the metamorphic grade is very low. These discrepancies in MDAs, metamorphism and deformation suggest that the Jayah Creek Metabasalt is not an equivalent unit to the ECVs and is an older unit. Based on the 1857 ± 5 Ma MDA, we suggest that most probably the Jayah Creek Metabasalt belongs to the units mapped as Post-Barramundi basement (Fig. 9). In contrast, the MDA of 1781 ± 15 Ma obtained for the Timothy Creek Sandstone is similar to the 1779 ± 4 Ma MDA determined for the Lena Quartzite (Neumann et al., 2006). The Lena Quartzite is hosted within the

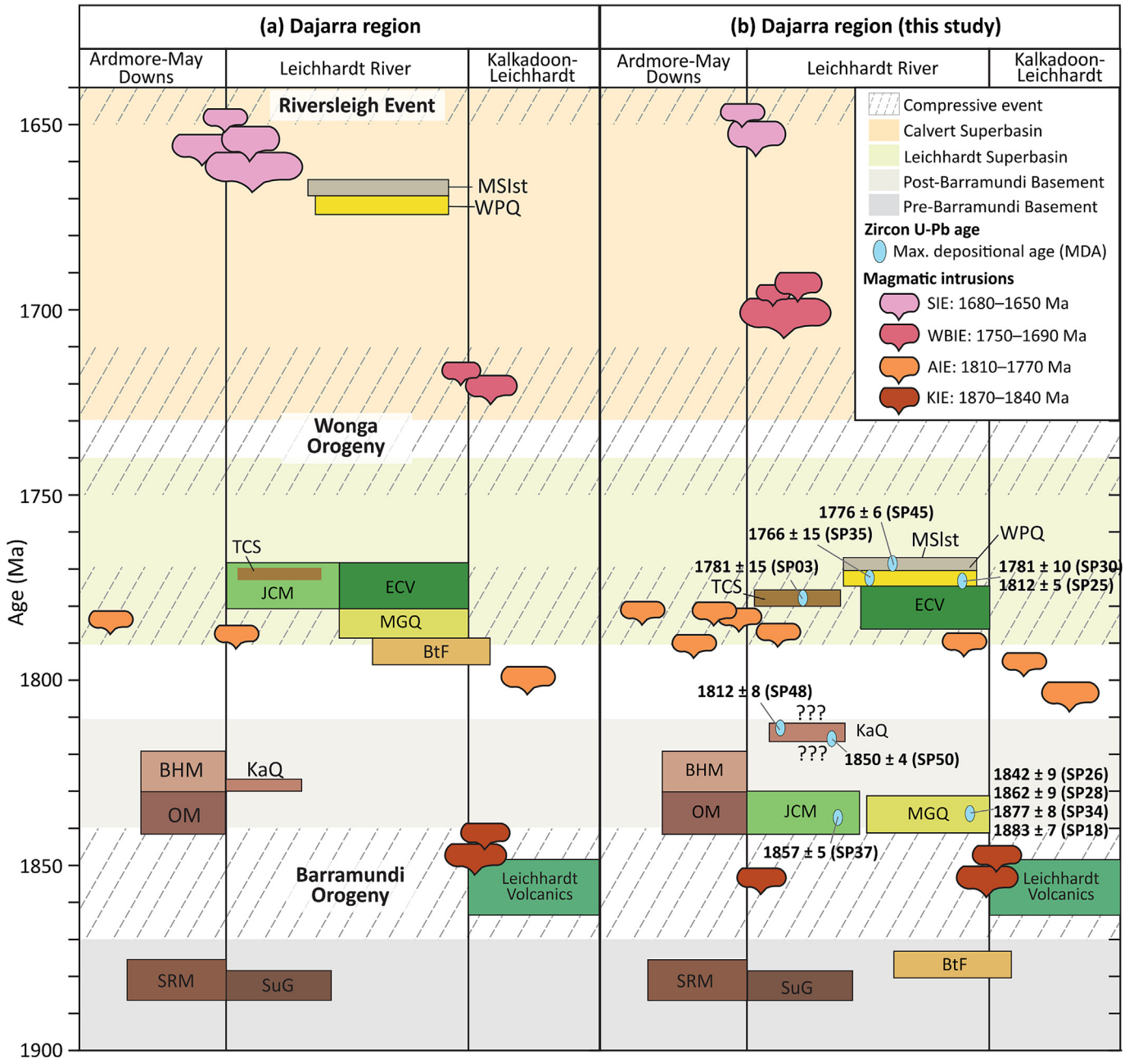

Fig. 9. Schematic diagram illustrating stratigraphic correlations of units in the Dajarra region (southern Western Succession). (a) Previously proposed correlations between stratigraphic units in the Dajarra region based on earlier studies. (b) Revised stratigraphic correlations for the Dajarra region incorporating new zircon U–Pb geochronological data from Noptalung et al. (2026) and this study. Unit abbreviations: BHM = Bucket Hole Metavolcanics, BtF = Bottletree Formation, ECV = Eastern Creek Volcanics, JCM = Jayah Creek Metabasalt, KaQ = Kallala Quartzite, MGQ = Mount Guide Quartzite, MSlst = Moondarra Siltstone, OM = Oroopo Metabasalt, SRM = Saint Ronans Metamorphics, SuG = Sulieman Gneiss, TCS = Timothy Creek Sandstone, WPQ = Warrina Park Quartzite, YM = Yaringa Metamorphics.

ECVs, whereas the Timothy Creek Sandstone unconformably overlies the Jayah Creek Metabasalt indicating that these two units share a temporal relationship but not a genetic one.

The stratigraphic position of Kallala Quartzite (Fig. 9) is uncertain and traditionally mapped as part of basement units (e.g. Blake et al., 1984; Blake, 1987). This was based on field relationships indicating an apparent gradational contact with the Sulieman Gneiss, concordant contact with Jayah Creek Metabasalt and intruded by the Sybella granites. Our two samples collected from Kallala Quartzite have MDAs of 1812 ± 8 Ma (SP48) and 1850 ± 4 Ma (SP50). The older sample (SP50) has a similar MDA to the younger sample (SP26) from Mount Guide Quartzite, but the two samples have very different detrital zircon distribution (Fig. 10) with populations older than 1900 Ma very poorly represented on both samples collected from the Kallala Quartzite suggesting a different source. Although the field relationships with Jayah Creek Metabasalt and the Sulieman Gneiss could not be confirmed, the recently reported intrusive age of ca. 1850 Ma (Noptalung et al., 2026) for the Sulieman Gneiss, together with much younger MDAs compared to the Jayah Creek Metabasalt, suggests that the Kallala Quartzite is unlikely to form part of the basement succession. Instead, it most likely represents early sedimentation stage during the initial opening of the Leichhardt Superbasin or forms part of the units mapped as Post Barramundi Basement.

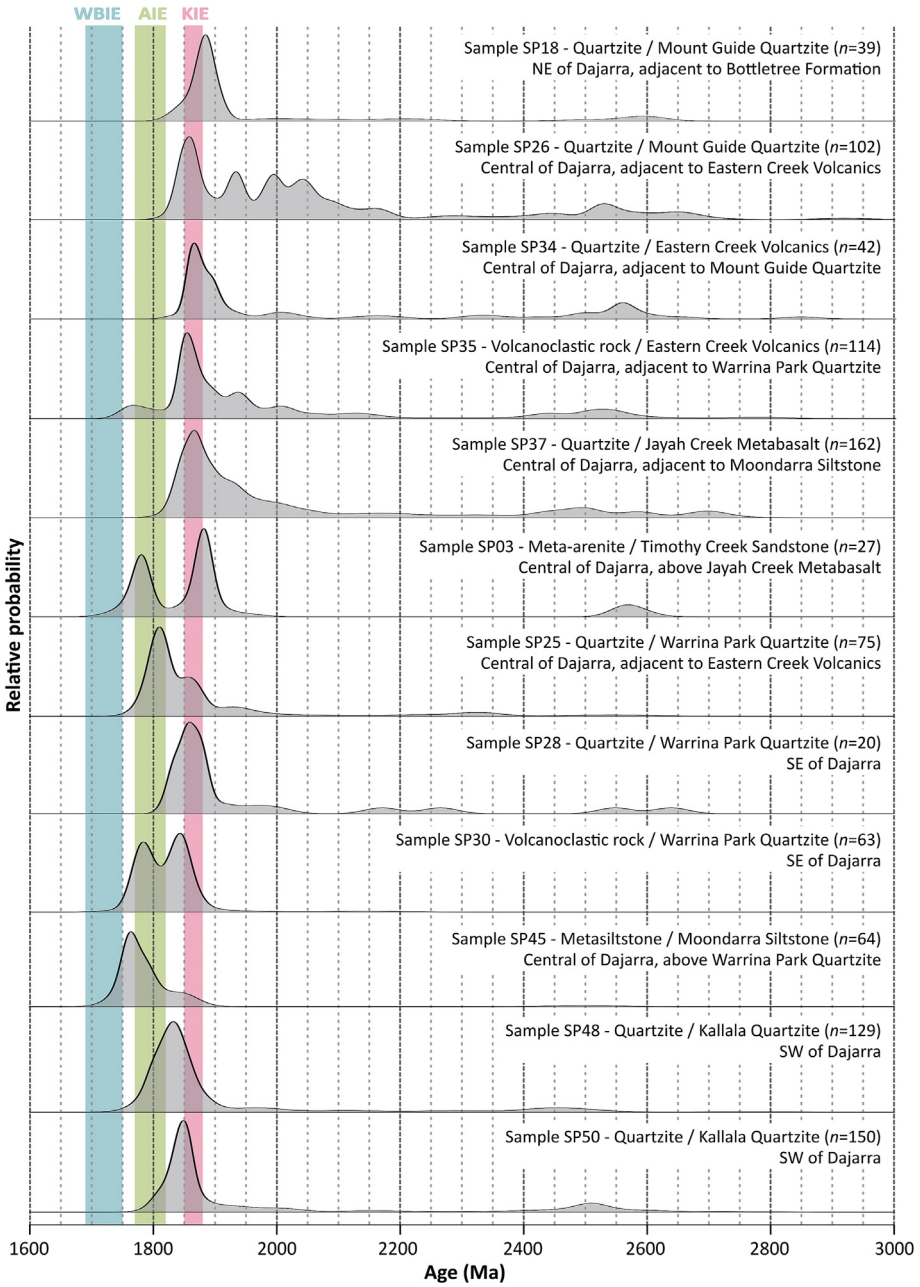

Fig. 10. Kernel density estimation of detrital zircon age populations in the Dajarra region. Vertical coloured bars in the background correspond to magmatic events that represent the likely Source for detrital zircons: KIE (Kalkadoon Igneous Event), AIE (Argylla Igneous Event) and WBIE (Wonga-Burstall Igneous Event) (Neumann et al., 2009a; Bultitude et al., 2021; Le et al., 2021b; Cocker et al., 2025; Noptalung et al., 2026).

Units mapped as part of Mount Isa Group (Warrina Park Quartzite and Moondarra Siltstone) have been interpreted to extend into the southern part of the WS, including undercover (e.g. Spampinato et al., 2015). Published MDAs from equivalent units in the northern part of the WS indicate depositional ages of ca. 1680 Ma for the Warrina Park Quartzite and the Moondarra Siltstone (Neumann et al., 2009b). In contrast, our U-Pb detrital zircon results yield significantly older MDAs of 1812 ± 5 Ma (SP25), 1862 ± 9 Ma (SP28) and 1781 ± 10 Ma (SP30) for the Warrina Park Quartzite and 1776 ± 6 Ma for the Moondarra Siltstone (SP45). The units mapped as Warrina Park Quartzite in the southern part of Dajarra region contain intercalated volcaniclastics (SP30) which constrains deposition of this unit at 1781 ± 10 Ma, which is almost identical to the MDA of 1776 ± 6 Ma obtained for the Moondarra Siltstone near the Wonomo Fault (Fig. 4a). These results suggest that the sedimentary units along the Wonomo Fault are unlikely to belong to the Mount Isa Group as defined in the northern part of the WS and their MDAs resemble closely the typical MDAs for units belonging to the early Leichhardt Superbasin sequences (Fig. 9).

5.2. Potential sources, crustal growth and tectonic evolution from Lu-Hf isotope systematics in zircons

5.2.1. The Dajarra region

The maximum depositional ages in the Dajarra region cluster in two age groups, an older one between ca. 1890 Ma and 1840 Ma and a younger one between ca. 1820 Ma and 1770 Ma (Table 1;

Fig. 10). These age groups correspond closely to igneous events defined by Noptalung et al. (2026), more precisely the KIE and the AIE. This suggests that the detrital zircons were locally derived and their Hf isotopic signature can be used as a proxy for the nature of the magmatism during these two major igneous events.

Detrital zircon $\varepsilon_{Hf}(t)$ values record the isotopic character of their parental melts but do not uniquely constrain the processes responsible for magma generation. Positive $\varepsilon_{Hf}(t)$ values indicate derivation from isotopically depleted reservoirs, whereas negative values reflect incorporation of enriched crustal components. However, such signatures may arise from multiple processes, including mantle-derived magma generation, crustal assimilation, remelting of older crust, or hybridisation between juvenile and evolved reservoirs. Consequently, $\varepsilon_{Hf}(t)$ values alone cannot discriminate unequivocally between juvenile addition and crustal reworking.

The older detrital population from the Dajarra region is dominated by unradiogenic to near-CHUR $\varepsilon_{Hf}(t)$ values (−4.7 to +2.2) indicating that the main mechanism of crustal growth during the Barramundi Orogeny and the associated KIE was dominated by reworking older crust with limited juvenile crust addition. This is consistent with Hf isotope signature from coeval igneous rocks (e.g. Bierlein et al., 2011; Lewis et al., 2022; Olierook et al., 2022; Noptalung et al., 2026). Extremely unradiogenic grains in this study ($\varepsilon_{Hf}(t)$ up to −13.1) match the Archean model ages documented beneath the southern Mount Isa Terrane by Olierook et al. (2022) and indicate the involvement of Archean crust, although no such crust has been identified yet in the region.

In contrast, the younger population (ca. 1820–1770 Ma) exhibits negative to strongly positive $\varepsilon_{Hf}(t)$ values (up to +8.7), suggesting juvenile crust addition during reworking of older crust. This reflects to mixing/assimilation processes, whereby juvenile melt interacted with older crust. The dataset of Noptalung et al. (2026) also indicates that some of the 1820–1780 Ma plutons in the Dajarra region have juvenile Hf peaks although most plutons are dominated by unradiogenic values. The datasets of Lewis et al. (2022), Bierlein et al. (2011) and Olierook et al. (2022) are dominated by unradiogenic $\varepsilon_{Hf}(t)$. This period corresponds to the emplacement of major mafic volcanic rocks forming the ECVs indicating that mantle-derived magmatism was present, although most plutonism was dominated by internal reworking of older crust. The eruption of the ECVs most likely indicates that some crustal thinning occurred, with heat advection from the mantle contributing to crustal melting and the emplacement of the AIE plutons.

5.2.2. Mount Isa Inlier and the eastern margin of the North Australia Craton

The available Lu-Hf isotope systematics in zircon grains from Mount Isa Inlier is summarised by Noptalung et al. (2026) and consists of Lu-Hf measurements on zircon grains separated from Proterozoic igneous rocks and sedimentary units derived mainly from the KLB and the WS. An important shortcoming of the Noptalung et al. (2026) dataset is the limited number of zircon grains younger than 1700 Ma.

The compiled dataset with the new data presented in this study is presented in Fig. 11. To quantify temporal variations in mantle versus crustal contributions and to make interpretations easier, we calculated a simple juvenile index (*JI*) for each 10 Ma time bin. The *JI* is defined as:

$$JI = \frac{NJ - NE}{N} = 2\left(\frac{NJ}{N}\right) - 1$$

where *NJ* is the number of zircon analyses with $\varepsilon_{Hf}(t) \geq 0$ (interpreted as juvenile, mantle-derived signatures), *NE* is the number with $\varepsilon_{Hf}(t) < 0$ (reworked crustal signatures), and *N* is the total number of analyses in each time bin. This dimensionless index ranges from −1 (wholly evolved crust) to +1 (entirely juvenile input), with 0 indicating equal juvenile and evolved contributions.

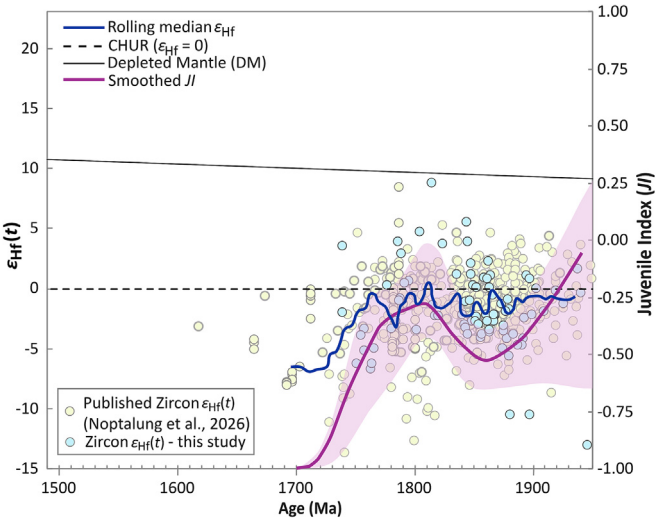

Fig. 11. $\varepsilon_{Hf}(t)$ datasets and calculated Juvenile Index (*JI*) values from magmatic and detrital zircons in the Mount Isa Inlier. Proterozoic magmatic and detrital Hf isotopic data (Bierlein et al., 2011; Lewis et al., 2022; Olierook et al., 2022) compiled by Noptalung et al. (2026).

The *JI* offers a transparent and reproducible way to summarise the balance between juvenile and evolved isotopic signatures without relying on arbitrary thresholding or subjective interpretation of $\varepsilon_{Hf}(t)$ scatter. When plotted alongside the rolling-median $\varepsilon_{Hf}(t)$ curve, the *JI* effectively highlights intervals of enhanced mantle addition versus periods dominated by deep crustal reworking. The *JI* is not intended as a direct measure of net crustal growth, but rather as a metric describing temporal variations in the relative proportion of isotopically depleted versus enriched zircon source components. We recognise that $\varepsilon_{Hf}(t)$ values alone cannot uniquely distinguish between juvenile mantle addition, crustal assimilation, or remelting of pre-existing crust, and that detrital zircon-based crustal growth models may be sensitive to interpretative assumptions (e.g., Pereira et al., 2024). Accordingly, the *JI* is used here as a comparative and internally consistent index to track isotopic source balance through time rather than as a quantitative estimate of continental growth.

To evaluate potential preservation bias, zircon U and Th concentrations were plotted against $\varepsilon_{Hf}(t)$ values. No systematic correlation was observed between U content and $\varepsilon_{Hf}(t)$, indicating that radiation damage or metamictization does not preferentially affect either juvenile or evolved Hf populations. This suggests that discordance filtering is unlikely to introduce systematic bias into the *JI* calculation. To quantify uncertainty in the *JI*, bootstrap resampling (n = 1000 iterations) was applied to each 10 Myr age bin. Confidence intervals (95%) were calculated from the resampled distributions and are shown as uncertainty bars in Fig. 11. These results demonstrate that observed temporal variations in *JI* exceed bin-level statistical uncertainty. A sensitivity analysis was conducted to assess the influence of the $\varepsilon_{Hf}(t)$ threshold on *JI* behaviour. *JI* was recalculated using thresholds of 0, +2, and +4 ε-units. Although absolute *JI* values vary slightly, the overall temporal trends remain stable, indicating that the interpretation of increased juvenile contribution during ca. 1820 Ma to 1780 Ma is not dependent on the chosen threshold.

The Noptalung et al. (2026) Hf zircon dataset displays an evolved $\varepsilon_{Hf}(t)$ range dominated by values between −10 and +2, with few analyses extending into clearly juvenile territory whereas the rolling median rarely rises above CHUR (Fig. 11). As a result, the

JI curve remains strongly negative or neutral through much of the interval, only approaching zero in the oldest bins. These patterns are consistent with derivation from isotopically depleted sources and suggest that the magmatic systems sampled in this dataset were largely derived from reworked crustal reservoirs.

The overall pattern between ca. 1900 Ma and 1700 Ma is decreasing juvenile input related to the KIE and the Barramundi Orogeny, increased juvenile input leading into the AIE and opening of the Leichhardt Superbasin followed by decreasing juvenile input with the onset of the Wonga Orogeny and the WBIE. Kohanpour et al. (2019) proposed that juvenile signals are observed during back-arc extension whereas evolved signatures dominate collisional settings. It is clear from both datasets that increased unradiogenic Hf dominates towards the final stages of the Barramundi Orogeny. However, the current tectonic models do not favour a collisional setting but rather invoke an Andean-style continental margin (e.g. Betts et al., 2016; Gibson et al., 2025) reworking an Archean lithospheric substrate (e.g. Bierlein et al., 2008; Olierook et al., 2022; Noptalung et al., 2026). The collision of the West Australian Craton (WAC) and the NAC at ca. 1830 Ma is documented in the Halls Creek Orogen (e.g. Griffin et al., 2000; Kohanpour et al., 2019) but no equivalent events are known from the eastern margin of the NAC, which instead is interpreted as a distal back-arc due to subduction retreat and slab rollback along the southern margin of the NAC (e.g. Giles et al., 2002; Betts and Giles, 2006). This is expressed in the Mount Isa Inlier as the opening of the Leichhardt Superbasin, extensive mafic magmatism and increased radiogenic Hf compositions. Thus, the increased juvenile input between ca. 1820 Ma and 1770 Ma is consistent with a back-arc setting, although the exact location of the subduction system is uncertain. The period corresponding to the Wonga Orogeny marks a pronounced decrease of juvenile input and increased crustal reworking. This period is synchronous with the proposed collision between the South Australian Craton (SAC) and the NAC (Payne et al., 2008; Reid et al., 2008; Reid and Hand, 2012). Although no collision was document along the eastern margin of the NAC at this time, the dominance of evolved Hf compositions during this time is consistent with a period of crustal shortening and orogenic activity.

To place the detrital zircon $\varepsilon_{Hf}(t)$ signatures into geological context, we compare them with published $\varepsilon_{Hf}(t)$ data from Paleoproterozoic igneous and *meta*-igneous rocks of the Dajarra–Mount Isa region (e.g., Olierook et al., 2022; Noptalung et al., 2026). The detrital zircon $\varepsilon_{Hf}(t)$ values overlap with those reported for I- and A-type granitoids emplaced between ca. 1880–1700 Ma. This correspondence suggests that these granitoid suites represent plausible sediment source regions and supports interpretation of sediment derivation within an active continental margin setting.

5.3. Tectonic setting from detrital zircons patterns – Intracratonic rifting or back arc extension during Leichhardt Superbasin formation

Most of the sedimentary units sampled in this study have MDAs indicating deposition post-Barramundi Orogeny or during the opening of the Leichhardt Superbasin. The tectonic setting of the Leichhardt Superbasin has been interpreted through two contrasting end-member models. Early structural and stratigraphic studies defined the basin as an intracratonic to intraplate rift system, based on *syn*-sedimentary faulting, half-graben architecture and stacked unconformity-bounded basin geometry (Glikson et al., 1976; Derrick, 1982; O'Dea et al., 1997a; Jackson et al., 2000; Gibson et al., 2016; Blaikie et al., 2017). In contrast, more recent studies based on plate-tectonic reconstructions proposed that the Leichhardt, together with the Calvert and Isa Superbasins, developed within a continental back-arc system generated in the overriding plate of a convergent margin linking basin formation to slab rollback, episodic basin inversion and progressive Nuna assembly (e.g. Giles et al., 2002; Betts and Giles, 2006; Gibson et al., 2020, 2025; Olierook et al., 2022).

Cawood et al. (2012) proposed that the difference between detrital zircons crystallization age (CA) and depositional age (DA) and the shape of the cumulative CA-DA curve can be used to distinguish the most likely tectonic setting in which the host sedimentary units were deposited. Detrital zircon grains deposited in a convergent setting/arc-back-arc basins will have a large proportion of zircons with CA≈DA (often ≥ 30%–40% of grains within 0–100 Ma of DA). The cumulative CA-DA curve for these zircon populations is very steep near 0 Ma, flattening only at larger lags. Detrital zircons deposited in a collisional setting/foreland basin setting will still have a significant population of young zircons but mixed with older basement ages, typically 10%–50% of grains within 0–150 Ma, then a broad tail of much older ages. Zircon grains deposited in extensional setting/intracratonic/passive margin basins will be dominated by old basement zircon grains with only a small tail of young grains, usually < 10% within 0–150 Ma and the cumulative curve is shallow from the origin.

The MDAs of the detrital populations from Dajarra region indicate that the sedimentary units in this part of Mount Isa Inlier formed pre or *syn*-Leichhardt Superbasin and the cumulative CA-DA curve can be used to infer the most likely tectonic setting during the formation of the Leichhardt Superbasin. All detrital zircon samples from Dajarra region have very steep curves near 0 Ma with 40%–50% of the grains within 0–100 Ma of DA consistent with a convergent setting/arc-back-arc basin (Fig. 12). The youngest zircon population in each sample closely matches the ages of synchronous magmatic events supporting synchronous magmatism and sedimentation typical for active continental margins. A similar pattern emerges from data presented by Olierook et al. (2022) that shows that zircon grains from metasedimentary units recovered from deep drilling undercover have MDAs that closely match the major peaks in magmatic activity and have minor Archean-Paleoproterozoic inheritance. A similar pattern emerges from detrital zircon analysed by Neumann et al. (2006, 2009b) in the northern part of the inlier suggesting an active continental margin

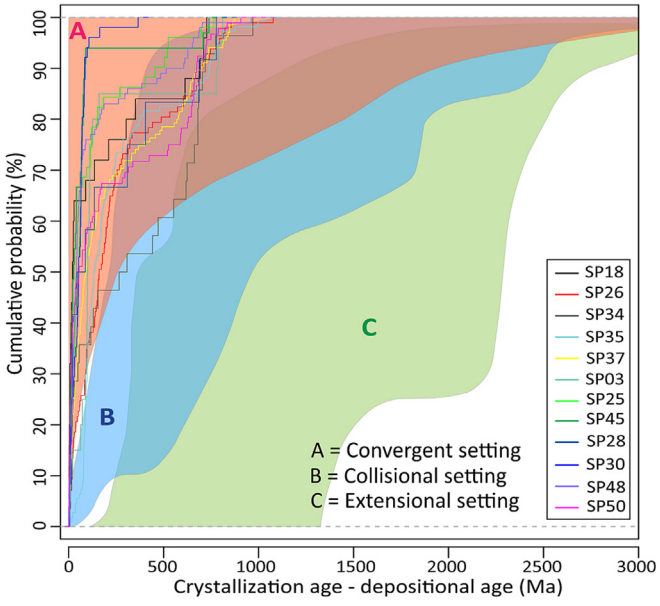

Fig. 12. Variation of the difference between the measured crystallization age for detrital zircon grains and depositional ages of metasedimentary rocks in Dajarra region, plotted as cumulative proportion curves, as a function of three main tectonic settings as proposed by Cawood et al. (2012).

setting as well. Our dataset does not contain detrital zircons from the Calvert and Isa superbasins sequences, but a review of data presented in Neumann et al. (2006, 2009b) clearly highlights a similar pattern with MDAs closely matching the age of synchronous igneous events and the deposition of the host sediments. These results are consistent with the Hf isotopic composition patterns discussed above and strongly suggest that not only the Leichhardt Superbasin formed along a convergent margin setting but the entire Mount Isa Inlier and the eastern margin of the NAC evolved along a long-lived active continental margin setting.

Although the CA-DA approach of Cawood et al. (2012) formally incorporates true depositional ages, we note that our analysis is based on MDAs. Because MDAs may slightly predate true sedimentation, this can introduce a minor systematic bias in cumulative age distributions. To address this, we evaluated our data following the approach outlined by Barham et al. (2022), which accounts for uncertainty in depositional age estimates when applying CA-DA discrimination. Using this modified framework, the Dajarra dataset plots consistently within the active continental margin field, characterised by a significant proportion of near-syndepositional zircons and limited lag times between crystallisation and deposition. We also acknowledge several methodological considerations in applying the CA-DA approach to this dataset. The majority of zircon crystallisation ages fall within a restricted Paleoproterozoic interval (ca. 2100–1700 Ma), and older grains are relatively scarce. Such limited temporal dispersion may reduce the sensitivity of cumulative curves to distinguish between convergent, collisional, and extensional settings. In addition, cumulative age spectra can be influenced by sediment-routing configuration, zircon fertility of source lithologies, recycling efficiency, and sedimentary sorting processes. Accordingly, CA-DA results are interpreted as probabilistic indicators of dominant source regimes rather than definitive basin-type diagnostics. The consistent classification of all samples within the convergent-margin field may partly reflect the methodological limitations discussed above. However, it may also carry tectonic significance. The persistence of convergent-margin cumulative spectra across intervals traditionally interpreted as pre-, syn-, and post-orogenic suggests that sediment supply to these basins remained dominated by arc-related and arc-derived crust throughout Paleoproterozoic evolution of the Mount Isa region. This raises the possibility that tectonic transitions in the area were less abrupt in terms of sediment routing and source-terrain dominance than implied by existing stratigraphic subdivisions. Accordingly, the CA-DA results may provide indirect evidence that convergent-margin processes exerted long-lived control on crustal architecture and sediment supply, even across intervals previously regarded as tectonically distinct. While this interpretation requires further testing, it highlights the potential for detrital zircon datasets to refine existing tectonic models rather than simply reproduce them.

6. Conclusion

U-Pb dating and Lu-Hf isotope analysis of metasedimentary rocks from the Dajarra region were undertaken to constrain maximum depositional ages, basin-forming tectonic settings, and the evolutionary history of continental crust in the southern Western Succession of the Mount Isa Inlier. Detrital zircons from these metasedimentary units yield older maximum depositional ages than equivalent stratigraphic units in the northern Western Succession. This discrepancy may reflect differences in the distribution and continuity of stratigraphic successions across the Western Succession, requiring refinement of the regional stratigraphic framework. Alternatively, the older depositional ages could indicate stronger input from older source regions into the southern sedimentary sequences. The detrital zircon record reveals a minor Neoarchean population (ca. 2600–2500 Ma) and dominant late Paleoproterozoic populations (ca. 1890–1840 Ma and ca. 1820–1750 Ma). Hf isotope compositions of Neoarchean zircons indicate reworking of older continental crust, potentially suggesting the presence of an Archean basement beneath the Mount Isa Inlier. By contrast, the late Paleoproterozoic populations record major episodes of crustal reworking and remelting between ca. 1890 Ma and 1840 Ma, with evidence for mixed sources involving both recycled older crust and juvenile mantle input during ca. 1820–1750 Ma. These late Paleoproterozoic zircon populations are contemporaneous with widespread magmatic activity recorded across the Mount Isa Inlier and the broader North Australian Craton (NAC). This supports interpretations that basin evolution and crustal growth during the late Paleoproterozoic were governed by subduction-related processes along an active continental margin of the NAC. Accordingly, the sedimentary successions of the southern Western Succession are best explained as deposits within a back-arc basin setting.

CRediT authorship contribution statement

Sutthida Noptalung: Writing – review & editing, Writing – original draft, Visualization, Validation, Resources, Methodology, Investigation, Formal analysis, Data curation. **Ioan V. Sanislav:** Writing – review & editing, Validation, Supervision, Funding acquisition, Conceptualization. **Helen A. Cocker:** Writing – review & editing. **Avish A. Kumar:** Writing – review & editing.

Declaration of competing interest

The authors declare that they have no known competing financial interests or personal relationships that could have appeared to influence the work reported in this paper.

Appendix A. Supplementary data

Supplementary data to this article can be found online at https://doi.org/10.1016/j.gsf.2026.102328.

References

Abu Sharib, A.S.A.A., Sanislav, I.V., 2013. Polymetamorphism accompanied switching in horizontal shortening during Isan Orogeny: example from the Eastern Fold Belt, Mount Isa Inlier, Australia. Tectonophysics 587, 146–167. https://doi.org/10.1016/j.tecto.2012.06.051.

Barham, M., Kirkland, C.L., Handoko, A.D., 2022. Understanding ancient tectonic settings through detrital zircon analysis. Earth Planet. Sci. Lett. 583, 117425. https://doi.org/10.1016/j.epsl.2022.117425.

Betts, P.G., 1999. Palaeoproterozoic mid-basin inversion in the northern Mt Isa terrane, Queensland. Aust. J. Earth Sci. 46, 735–748. https://doi.org/10.1046/j.1440-0952.1999.00741.x.

Betts, P.G., Armit, R.J., Stewart, J., Aitken, A.R.A., Ailleres, L., Donchak, P., Hutton, L., Withnall, I., Giles, D., 2016. Australia and Nuna. Geol. Soc. Lond. Spec. Publ. 424, 47–81. https://doi.org/10.1144/SP424.2.

Betts, P.G., Giles, D., 2006. The 1800–1100 Ma tectonic evolution of Australia. Precambrian Res. 144, 92–125. https://doi.org/10.1016/j.precamres.2005.11.006.

Betts, P.G., Giles, D., Mark, G., Lister, G.S., Goleby, B.R., Aillères, L., 2006. Synthesis of the Proterozoic evolution of the Mt Isa Inlier. Aust. J. Earth Sci. 53, 187–211. https://doi.org/10.1080/08120090500434625.

Betts, P.G., Lister, G.S., O'Dea, M.G., 1998. Asymmetric extension of the Middle Proterozoic lithosphere, Mount Isa terrane, Queensland, Australia. Tectonophysics 296, 293–316. https://doi.org/10.1016/S0040-1951(98)00144-9.

Bierlein, F.P., Black, L.P., Hergt;, J., Mark, G., 2008. Evolution of Pre-1.8 Ga basement rocks in the western Mt Isa Inlier, northeastern Australia—Insights from SHRIMP U–Pb dating and *in-situ* Lu–Hf analysis of zircons. Precambrian Res. 163, 159–173. https://doi.org/10.1016/j.precamres.2007.08.017.

Bierlein, F.P., Maas, R., Woodhead, J., 2011. Pre-1.8 Ga tectono-magmatic evolution of the Kalkadoon–Leichhardt Belt: implications for the crustal architecture and

metallogeny of the Mount Isa Inlier, northwest Queensland, Australia. Aust. J. Earth Sci. 58, 887–915. https://doi.org/10.1080/08120099.2011.571286.
Black, L.P., Kamo, S.L., Allen, C.M., Aleinikoff, J.N., Davis, D.W., Korsch, R.J., Foudoulis, C., 2003. TEMORA 1: a new zircon standard for Phanerozoic U–Pb geochronology. Chem. Geol. 200, 155–170. https://doi.org/10.1016/S0009-2541(03)00165-7.
Blaikie, T.N., Betts, P.G., Armit, R.J., Ailleres, L., 2017. The ca. 1740–1710 Ma Leichhardt Event: Inversion of a continental rift and revision of the tectonic evolution of the North Australian Craton. Precambrian Res. 292, 75–92. https://doi.org/10.1016/j.precamres.2017.02.003.
Blake, D.H., 1987. Geology of the Mount Isa Inlier and environs, Queensland and Northern Territory. Bur. Miner. Resour. Geol. Geophys. Aust. Bull. 225, 1–83.
Blake, D.H., 1986. Middle Proterozoic evolution of the Mt Isa Inlier, north-western Queensland, Australia: a synthesis. South Afr. J. Geol. 89, 253–262. https://doi.org/10.10520/EJC-1bb4fbcf12.
Blake, D.H., 1980. The early geological history of the Proterozoic Mount Isa Inlier, northwestern Queensland: an alternative interpretation. BMR J. Aust. Geol. Geophys. 5, 243–256.
Blake, D.H., Bultitude, R.J., Donchak, P.J.T., 1982. Dajarra 1:100000 Geological Map Commentary. Bureau of Mineral Resources, Geology, Geophysics, Canberra.
Blake, D.H., Bultitude, R.J., Donchak, P.J.T., Wyborn, L.A.I., Hone, I.G., 1984. Geology of the Duchess-Urandangi Region, Mount Isa Inlier, Queensland. Bureau of Mineral Resources, Geology and Geophysics, Canberra 219, 1–91.
Blake, D.H., Stewart, A.J., 1992. Stratigraphic and tectonic framework, Mount Isa Inlier. In: Stewart, A.J., Blake, D.H. (Eds.), Detailed Studies of the Mount Isa Inlier. Australian Geological Survey Organisation Bulletin, Canberra, vol. 243, pp. 1–11.
Bouvier, A., Vervoort, J.D., Patchett, P.J., 2008. The Lu–Hf and Sm–Nd isotopic composition of CHUR: Constraints from unequilibrated chondrites and implications for the bulk composition of terrestrial planets. Earth Planet. Sci. Lett. 273, 48–57. https://doi.org/10.1016/j.epsl.2008.06.010.
Bradshaw, B.E., Lindsay, J.F., Krassay, A.A., Wells, A.T., 2000. Attenuated basin-margin sequence stratigraphy of the Palaeoproterozoic Calvert and Isa Superbasins: the Fickling Group, southern Murphy Inlier, Queensland. Aust. J. Earth Sci. 47, 599–623. https://doi.org/10.1046/j.1440-0952.2000.00794.x.
Brown, A., Spandler, C., Blenkinsop, T.G., 2023. New age constraints for the Tommy Creek Domain of the Mount Isa Inlier, Australia. Aust. J. Earth Sci. 70, 358–374. https://doi.org/10.1080/08120099.2023.2171124.
Bultitude, R.J., 1982. Ardmore 1:100000 Geological Map Commentary. Bureau of Mineral Resources, Geology, Geophysics, Canberra.
Bultitude, R.J., Purdy, D.J., Brown, D.D., Hoy, D., 2021. Igneous Geology of the Mary Kathleen Domain (MKD) (GSQ Record No. 2021/02). Geological Survey of Queensland, Brisbane.
Carson, C.J., Hutton, L.J., Withnall, I.W., Perkins, W.G., 2009. Joint GSQ-GA NGA Geochronology Project, Mount Isa Region, 2007–2008 (GSQ Record No. 2008/05). Geological Survey of Queensland, Brisbane.
Carson, C.J., Hutton, L.J., Withnall, I.W., Perkins, W.J., Donchak, P.J.T., Parsons, A., Blake, P.R., Sweet, I.P., Neumann, N.L., Lambeck, A., 2011. Joint GSQ-GA NGA geochronology Project, Mount Isa Region, 2009–2010 (GSQ Record No. 2011/03). Geological Survey of Queensland, Brisbane.
Cawood, P.A., Hawkesworth, C.J., Dhuime, B., 2012. Detrital zircon record and tectonic setting. Geology 40, 875–878. https://doi.org/10.1130/G32945.1.
Cawood, P.A., Nemchin, A.A., Strachan, R., Prave, T., Krabbendam, M., 2007. Sedimentary basin and detrital zircon record along East Laurentia and Baltica during assembly and breakup of Rodinia. J. Geol. Soc. 164, 257–275. https://doi.org/10.1144/0016-76492006-115.
Cocker, H.A., Sanislav, I., Dirks, P., McCoy-West, A., 2025. Zircon U–Pb emplacement ages of intrusions in the Mary Kathleen Domain, Mount Isa Inlier, Australia. Aust. J. Earth Sci. 72 (4), 503–527. https://doi.org/10.1080/08120099.2025.2527816.
Connors, K.A., Page, R.W., 1995. Relationships between magmatism, metamorphism and deformation in the western Mount Isa Inlier, Australia. Precambrian Res. 71, 131–153. https://doi.org/10.1016/0301-9268(94)00059-Z.
de Vries, S.T., Pryer, L.L., Fry, N., 2008. Evolution of Neoarchaean and Proterozoic basins of Australia. Precambrian Res. 166, 39–53. https://doi.org/10.1016/j.precamres.2008.01.005.
Derrick, G.M., 1982. A Proterozoic rift zone at Mount Isa, Queensland, and implications for mineralisation. BMR J. Aust. Geol. Geophys. 7, 81–92.
Derrick, G.M., Wilson, I.H., Hill, R.M., 1976. Revision of stratigraphic nomenclature in the Precambrian of northwestern Queensland. II: Haslingden Group. Qld. Gov. Min. J. 77, 300–306.
Domagala, J., Southgate, P.N., McConachie, B.A., Pidgeon, B.A., 2000. Evolution of the Palaeoproterozoic Prize, Gun and lower Loretta Supersequences of the Surprise Creek Formation and Mt Isa Group. Aust. J. Earth Sci. 47, 485–507. https://doi.org/10.1046/j.1440-0952.2000.00796.x.
Eriksson, K.A., Simpson, E.L., 1993. Siliciclastic braided-alluvial sediments intercalated within continental flood basalts in the early to middle Proterozoic Mount Isa Inlier, Australia. In: Marzo, M., Puigdefábregas, C. (Eds.), Alluvial Sedimentation. Special Publication No. 17 of the International Association of Sedimentologists, Blackwell Scientific Publications, Oxford, pp. 473–488.
Etheridge, M.A., Rutland, R.W.R., Wyborn, L.A., 1987. Orogenesis and tectonic process in the Early to Middle Proterozoic of northern Australia. In: Kröner, A. (Ed.), Proterozic Lithospheric Evolution, Geodynamics Series. American Geophysical Union, Washington, pp. 131–147.
Foster, D.R.W., Austin, J.R., 2008. The 1800–1610 Ma stratigraphic and magmatic history of the Eastern Succession, Mount Isa Inlier, and correlations with adjacent Paleoproterozoic terranes. Precambrian Res. 163, 7–30. https://doi.org/10.1016/j.precamres.2007.08.010.
Gehrels, G., 2014. Detrital zircon U-Pb geochronology applied to tectonics. Annu. Rev. Earth Planet. Sci. 42, 127–149. https://doi.org/10.1146/annurev-earth-050212-124012.
Geological Survey of Queensland, 2011. Proterozoic geological domains. In: North-West Queensland Mineral and Energy Province Report. Queensland Department of Employment, Economic Development and Innovation, Brisbane, pp. 6–22.
Gibson, G.M., Champion, D.C., Doublier, M.P., 2025. The Paleoproterozoic Trans-Australian Orogen: its magmatic and tectonothermal record, links to northern Laurentia, and implications for supercontinent assembly. GSA Bull. 137, 495–521. https://doi.org/10.1130/B36255.1.
Gibson, G.M., Champion, D.C., Huston, D.L., Withnall, I.W., 2020. Orogenesis in Paleo-Mesoproterozoic eastern Australia: a response to arc-continent and continent-continent collision during assembly of the Nuna supercontinent. Tectonics 39, e2019TC005717. https://doi.org/10.1029/2019TC005717.
Gibson, G.M., Meixner, A.J., Withnall, I.W., Korsch, R.J., Hutton, L.J., Jones, L.E.A., Holzschuh, J., Costelloe, R.D., Henson, P.A., Saygin, E., 2016. Basin architecture and evolution in the Mount Isa mineral province, northern Australia: Constraints from deep seismic reflection profiling and implications for ore genesis. Ore Geol. Rev. 76, 414–441. https://doi.org/10.1016/j.oregeorev.2015.07.013.
Giles, D., Betts, P., Lister, G., 2002. Far-field continental backarc setting for the 1.80–1.67 Ga basins of northeastern Australia. Geology 30, 823–826. https://doi.org/10.1130/0091-7613(2002)030%253C0823:FFCBSF%253E2.0.CO;2.
Glikson, A.Y., Derrick, G.M., Wilson, I.H., Hill, R.M., 1976. Tectonic evolution and crustal setting of the middle Proterozoic Leichhardt River fault trough, Mount Isa region, northwestern Queensland. BMR J. Aust. Geol. Geophys. 1, 115–129.
Griffin, T.J., Page, R.W., Sheppard, S., Tyler, I.M., 2000. Tectonic implications of Palaeoproterozoic post-collisional, high-K felsic igneous rocks from the Kimberley region of northwestern Australia. Precambrian Res. 101, 1–23. https://doi.org/10.1016/S0301-9268(99)00084-4.
Hawkesworth, C.J., Dhuime, B., Pietranik, A.B., Cawood, P.A., Kemp, A.I.S., Storey, C. D., 2010. The generation and evolution of the continental crust. J. Geol. Soc. 167, 229–248. https://doi.org/10.1144/0016-76492009-072.
Hawkesworth, C.J., Kemp, A.I.S., 2006. Using hafnium and oxygen isotopes in zircons to unravel the record of crustal evolution. Chem. Geol. 226, 144–162. https://doi.org/10.1016/j.chemgeo.2005.09.018.
Horstwood, M.S.A., Košler, J., Gehrels, G., Jackson, S.E., McLean, N.M., Paton, C., Pearson, N.J., Sircombe, K., Sylvester, P., Vermeesch, P., Bowring, J.F., Condon, D. J., Schoene, B., 2016. Community-derived standards for LA-ICP-MS U-(Th-)Pb geochronology – uncertainty propagation, age interpretation and data reporting. Geostand. Geoanal. Res. 40, 311–332. https://doi.org/10.1111/j.1751-908X.2016.00379.x.
Iaccheri, L.M., 2019. Composite basement along the southern margin of the North Australian Craton: evidence from in-situ zircon U-Pb-O-Hf and whole-rock Nd isotopic compositions. Lithos 324–325, 733–746. https://doi.org/10.1016/j.lithos.2018.11.006.
Jackson, M., Southgate, P., Black, L., Blake, P., Domagala, J., 2005. Overcoming Proterozoic quartzite sand-body miscorrelations: integrated sequence stratigraphy and SHRIMP U–Pb dating of the Surprise Creek Formation, Torpedo Creek and Warrina Park Quartzites, Mt Isa Inlier. Aust. J. Earth Sci. 52, 1–25. https://doi.org/10.1080/08120090500039390.
Jackson, M.J., Scott, D.L., Rawlings, D.J., 2000. Stratigraphic framework for the Leichhardt and Calvert Superbasins: review and correlations of the pre-1700 Ma successions between Mt Isa and McArthur River. Aust. J. Earth Sci. 47, 381–403. https://doi.org/10.1046/j.1440-0952.2000.00789.x.
Kemp, A.I.S., Foster, G.L., Scherstén, A., Whitehouse, M.J., Darling, J., Storey, C., 2009. Concurrent Pb–Hf isotope analysis of zircon by laser ablation multi-collector ICP-MS, with implications for the crustal evolution of Greenland and the Himalayas. Chem. Geol. 261, 244–260. https://doi.org/10.1016/j.chemgeo.2008.06.019.
Kohanpour, F., Kirkland, C.L., Gorczyk, W., Occhipinti, S., Lindsay, M.D., Mole, D., Le Vaillant, M., 2019. Hf isotopic fingerprinting of geodynamic settings: Integrating isotopes and numerical models. Gondwana Res. 73, 190–199. https://doi.org/10.1016/j.gr.2019.03.017.
Krassay, A.A., Bradshaw, B.E., Domagala, J., Jackson, M.J., 2000. Siliciclastic shoreline to growth-faulted, turbiditic sub-basins: the Proterozoic River Supersequence of the upper McNamara Group on the Lawn Hill Platform, northern Australia. Aust. J. Earth Sci. 47, 533–562. https://doi.org/10.1046/j.1440-0952.2000.00790.x.
Lancaster, P.J., Storey, C.D., Hawkesworth, C.J., Dhuime, B., 2011. Understanding the roles of crustal growth and preservation in the detrital zircon record. Earth Planet. Sci. Lett. 305, 405–412. https://doi.org/10.1016/j.epsl.2011.03.022.
Le, T.X., Dirks, P.H.G.M., Sanislav, I.V., Huizenga, J.M., Cocker, H.A., Manestar, G.N., 2021a. Geological setting and mineralization characteristics of the Tick Hill Gold Deposit, Mount Isa Inlier, Queensland. Australia. Ore Geol. Rev. 137, 104288. https://doi.org/10.1016/j.oregeorev.2021.104288.
Le, T.X., Dirks, P.H.G.M., Sanislav, I.V., Huizenga, J.M., Cocker, H.A., Manestar, G.N., 2021b. Geochronological constraints on the geological history and gold mineralization in the Tick Hill region. Mt Isa Inlier. Precambrian Res. 366, 106422. https://doi.org/10.1016/j.precamres.2021.106422.
Le, T.X., Dirks, P.H.G.M., Sanislav, I.V., Huizenga, J.M., Cocker, H.A., Nguyen, G.T.T., 2024. *P – T* conditions of metamorphic and hydrothermal events at Tick Hill

gold deposit, Mount Isa, Queensland. Australia. Aust. J. Earth Sci. 71, 538–552. https://doi.org/10.1080/08120099.2024.2320195.
Lewis, C.J., Bultitude, R.J., Hutton, L.J., Waltenberg, K., Armstrong, R.A., Evans, N.J., 2022. Unravelling the pre-1860–1850 Ma 'basement' history of the Mount Isa Inlier. Queensland Geol. Surv. Rec. 2022 (2), 1–50.
MacCready, T., Goleby, B.R., Goncharov, A., Drummond, B.J., Lister, G.S., 1998. A framework of overprinting orogens based on interpretation of the Mount Isa deep seismic transect. Econ. Geol. 93, 1422–1434. https://doi.org/10.2113/gsecongeo.93.8.1422.
Magee, C.W., Withnall, I.W., Hutton, L.J., Perkins, W.J., Donchak, P.J.T., Parson, A., Blake, P.R., Sweet, I.P., Carson, C.J., 2012. Joint GSQ–GA geochronology project, Mount Isa Region, 2008–2009 (GSQ Record No. 2012/07). Geological Survey of Queensland, Brisbane.
Neumann, N.L., Gibson, G.M., Southgate, P.N., 2009a. New SHRIMP age constraints on the timing and duration of magmatism and sedimentation in the Mary Kathleen Fold Belt, Mt Isa Inlier, Australia. Aust. J. Earth Sci. 56, 965–983. https://doi.org/10.1080/08120090903005410.
Neumann, N.L., Southgate, P.N., Gibson, G.M., 2009b. Defining unconformities in Proterozoic sedimentary basins using detrital geochronology and basin analysis—An example from the Mount Isa Inlier, Australia. Precambrian Res. 168, 149–166. https://doi.org/10.1016/j.precamres.2008.09.012.
Neumann, N.L., Southgate, P.N., Gibson, G.M., MCintyre, A., 2006. New SHRIMP geochronology for the Western Fold Belt of the Mt Isa Inlier: developing a 1800–1650 Ma event framework. Aust. J. Earth Sci. 53, 1023–1039. https://doi.org/10.1080/08120090600923287.
Noptalung, S., Sanislav, I.V., Cocker, H.A., Kumar, A., 2026. Zircon U-Pb ages and Lu-Hf isotopic systematics in granites from Mt Isa Inlier – evidence of prolonged reworking of an active continental margin during the final assembly of the Nuna (Columbia) supercontinent. Precambrian Res. 432, 107965. https://doi.org/10.1016/j.precamres.2025.107965.
O'Dea, M.G., Lister, G.S., Betts, P.G., Pound, K.S., 1997a. A shortened intraplate rift system in the Proterozoic Mount Isa terrane, NW Queensland, Australia. Tectonics 16, 425–441. https://doi.org/10.1029/96TC03276.
O'Dea, M.G., Lister, G.S., Maccready, T., Betts, P.G., Oliver, N.H.S., Pound, K.S., Huang, W., Valenta, R.K., 1997b. Geodynamic evolution of the Proterozoic Mount Isa terrain. Geol. Soc. Lond. Spec. Publ. 121, 99–122. https://doi.org/10.1144/GSL.SP.1997.121.01.05.
Olierook, H.K.H., Mervine, E.M., Armstrong, R., Duckworth, R., Evans, N.J., McDonald, B., Kirkland, C.L., Shantha Kumara, A., Wood, D.G., Cristall, J., Jhala, K., Stirling, D. A., Friedman, I., McInnes, B.I.A., 2022. Uncovering the Leichhardt Superbasin and Kalkadoon-Leichhardt complex in the southern Mount Isa Terrane, Australia. Precambrian Res. 375, 106680. https://doi.org/10.1016/j.precamres.2022.106680.
Paces, J.B., Miller Jr., J.D., 1993. Precise U-Pb ages of Duluth complex and related mafic intrusions, northeastern Minnesota: Geochronological insights to physical, petrogenetic, paleomagnetic, and tectonomagmatic processes associated with the 1.1 Ga Midcontinent Rift System. J. Geophys. Res. Solid Earth 98, 13997–14013. https://doi.org/10.1029/93JB01159.
Page, R.W., 1988. Geochronology of early to middle Proterozoic fold belts in northern Australia: a review. Precambrian Res. 40–41, 1–19. https://doi.org/10.1016/0301-9268(88)90058-7.
Page, R.W., Jackson, M.J., Krassay, A.A., 2000. Constraining sequence stratigraphy in north Australian basins: SHRIMP U–Pb zircon geochronology between Mt Isa and McArthur River. Aust. J. Earth Sci. 47, 431–459. https://doi.org/10.1046/j.1440-0952.2000.00797.x.
Page, R.W., Sweet, I.P., 1998. Geochronology of basin phases in the western Mt Isa Inlier, and correlation with the McArthur Basin. Aust. J. Earth Sci. 45, 219–232. https://doi.org/10.1080/08120099808728383.
Page, R.W., Williams, I.S., 1988. Age of the barramundi orogeny in northern Australia by means of ion microprobe and conventional U-Pb zircon studies. Precambrian Res. 40–41, 21–36. https://doi.org/10.1016/0301-9268(88)90059-9.
Paton, C., Hellstrom, J., Paul, B., Woodhead, J., Hergt, J., 2011. Iolite: Freeware for the visualisation and processing of mass spectrometric data. J. Anal. at. Spectrom. 26, 2508. https://doi.org/10.1039/c1ja10172b.
Payne, J.L., Hand, M., Barovich, K.M., Wade, B.P., 2008. Temporal constraints on the timing of high-grade metamorphism in the northern Gawler Craton: implications for assembly of the Australian Proterozoic. Aust. J. Earth Sci. 55, 623–640. https://doi.org/10.1080/08120090801982595.
Pereira, F.S., Lafon, J.-M., Rosa, M. de L. da S., Conceição, H., Bertotti, A.L., Milhomem Neto, J.M., Lana, C., Koester, E., 2024. Constraints on the source and petrogenesis of early Ediacaran shoshonitic mafic magmatism and high-K calc-alkaline granitoids in the Sergipano Orogenic System, Borborema Province, Brazil. Precambrian Res. 404, 107312. doi: 10.1016/j.precamres.2024.107312.
Reid, A.J., Hand, M., 2012. Mesoarchean to Mesoproterozoic evolution of the southern Gawler Craton, South Australia. Episodes 35, 216–225. https://doi.org/10.18814/epiiugs/2012/v35i1/021.
Reid, A.J., McAvaney, S.O., Fraser, G.L., 2008. Nature of the Kimban Orogeny across northern Eyre Peninsula. MESA J. 51, 25–34.
Sanislav, I.V., Blenkinsop, T.G., Dirks, P.H.G.M., 2018. Archaean crustal growth through successive partial melting events in an oceanic plateau-like setting in the Tanzania Craton. Terra Nova 30, 169–178. https://doi.org/10.1111/ter.12323.
Sanislav, I.V., Wormald, R.J., Dirks, P.H.G.M., Blenkinsop, T.G., Salamba, L., Joseph, D., 2014. Zircon U–Pb ages and Lu–Hf isotope systematics from late-tectonic granites, Geita Greenstone Belt: Implications for crustal growth of the Tanzania Craton. Precambrian Res. 242, 187–204. https://doi.org/10.1016/j.precamres.2013.12.026.
Scott, D.L., Rawlings, D.J., Page, R.W., Tarlowski, C.Z., Idnurm, M., Jackson, M.J., Southgate, P.N., 2000. Basement framework and geodynamic evolution of the Palaeoproterozoic superbasins of north-central Australia: an integrated review of geochemical, geochronological and geophysical data. Aust. J. Earth Sci. 47, 341–380. https://doi.org/10.1046/j.1440-0952.2000.00793.x.
Söderlund, U., Patchett, P.J., Vervoort, J.D., Isachsen, C.E., 2004. The ^{176}Lu decay constant determined by Lu–Hf and U–Pb isotope systematics of Precambrian mafic intrusions. Earth Planet. Sci. Lett. 219, 311–324. https://doi.org/10.1016/S0012-821X(04)00012-3.
Southgate, P.N., Bradshaw, B.E., Domagala, J., Jackson, M.J., Idnurm, M., Krassay, A.A., Page, R.W., Sami, T.T., Scott, D.L., Lindsay, J.F., McConachie, B.A., Tarlowski, C., 2000. Chronostratigraphic basin framework for Palaeoproterozoic rocks (1730–1575 Ma) in northern Australia and implications for base-metal mineralisation. Aust. J. Earth Sci. 47, 461–483. https://doi.org/10.1046/j.1440-0952.2000.00787.x.
Spampinato, G.P.T., Betts, P.G., Ailleres, L., Armit, R.J., 2015. Structural architecture of the southern Mount Isa terrane in Queensland inferred from magnetic and gravity data. Precambrian Res. 269, 261–280. https://doi.org/10.1016/j.precamres.2015.08.017.
Spence, J.S., Sanislav, I.V., Dirks, P.H.G.M., 2022. Evidence for a 1750–1710 Ma orogenic event, the Wonga Orogeny, in the Mount Isa Inlier, Australia: Implications for the tectonic evolution of the North Australian Craton and Nuna Supercontinent. Precambrian Res. 369, 106510. https://doi.org/10.1016/j.precamres.2021.106510.
Spence, J.S., Sanislav, I.V., Dirks, P.H.G.M., 2021. 1750–1710 Ma deformation along the eastern margin of the North Australia Craton. Precambrian Res. 353, 106019. https://doi.org/10.1016/j.precamres.2020.106019.
Spencer, C.J., Kirkland, C.L., Roberts, N.M.W., Evans, N.J., Liebmann, J., 2020. Strategies towards robust interpretations of *in situ* zircon Lu–Hf isotope analyses. Geosci. Front. 11, 843–853. https://doi.org/10.1016/j.gsf.2019.09.004.
Spencer, C.J., Kirkland, C.L., Taylor, R.J.M., 2016. Strategies towards statistically robust interpretations of *in situ* U–Pb zircon geochronology. Geosci. Front. 7, 581–589. https://doi.org/10.1016/j.gsf.2015.11.006.
Tichomirowa, M., Käßner, A., Sperner, B., Lapp, M., Leonhardt, D., Linnemann, U., Münker, C., Ovtcharova, M., Pfänder, J.A., Schaltegger, U., Sergeev, S., von Quadt, A., Whitehouse, M., 2019. Dating multiply overprinted granites: the effect of protracted magmatism and fluid flow on dating systems (zircon U-Pb: SHRIMP/SIMS, LA-ICP-MS, CA-ID-TIMS; and Rb–Sr, Ar–Ar) – Granites from the Western Erzgebirge (Bohemian Massif, Germany). Chem. Geol. 519, 11–38. https://doi.org/10.1016/j.chemgeo.2019.04.024.
Tomson, J.K., Amal Dev, J., 2024. Detrital zircon U-Pb ages and Hf isotopes of quartzites from Southern Granulite Terrane, India: Implications for the Precambrian crustal evolution and paleogeography. Precambrian Res. 404, 107348. https://doi.org/10.1016/j.precamres.2024.107348.
Vermeesch, P., 2021. Maximum depositional age estimation revisited. Geosci. Front. 12, 843–850. https://doi.org/10.1016/j.gsf.2020.08.008.
Vermeesch, P., 2018. IsoplotR: a free and open toolbox for geochronology. Geosci. Front. 9, 1479–1493. https://doi.org/10.1016/j.gsf.2018.04.001.
Vervoort, J.D., Blichert-Toft, J., 1999. Evolution of the depleted mantle: Hf isotope evidence from juvenile rocks through time. Geochim. Cosmochim. Acta 63, 533–556. https://doi.org/10.1016/S0016-7037(98)00274-9.
Wang, L.-J., Griffin, W.L., Yu, J.-H., O'Reilly, S.Y., 2013. U–Pb and Lu–Hf isotopes in detrital zircon from Neoproterozoic sedimentary rocks in the northern Yangtze Block: Implications for Precambrian crustal evolution. Gondwana Res. 23, 1261–1272. https://doi.org/10.1016/j.gr.2012.04.013.
Wilson, C.J.L., 1975. Structural features west of Mount Isa. J. Geol. Soc. Aust. 22, 457–476. https://doi.org/10.1080/00167617508728911.
Withnall, I.W., Hutton, L.J., 2013. North Australian Craton. In: Jell, P.A. (Ed.), Geology of Queensland. Geological Survey of Queensland, Brisbane, pp. 23–112.
Woodhead, J.D., Hergt;, J.M., 2005. A preliminary appraisal of seven natural zircon reference materials for in situ Hf isotope determination. Geostand. Geoanal. Res. 29, 183–195. https://doi.org/10.1111/j.1751-908X.2005.tb00891.x.
Wyborn, L., 1998. Younger ca 1500 Ma granites of the Williams and Naraku Batholiths, Cloncurry district, eastern Mt Isa Inlier: Geochemistry, origin, metallogenic significance and exploration indicators. Aust. J. Earth Sci. 45. https://doi.org/10.1080/08120099808728400.
Wyborn, L.A.I., 1988. Petrology, geochemistry and origin of a major Australian 1880-1840 Ma felsic volcano-plutonic suite: a model for intracontinental felsic magma generation. Precambrian Res. 40–41, 37–60. https://doi.org/10.1016/0301-9268(88)90060-5.
Wyborn, L.A.I., Page, R.W., McCulloch, M.T., 1988. Petrology, geochronology and isotope geochemistry of the post-1820 Ma granites of the Mount Isa Inlier: mechanisms for the generation of Proterozoic anorogenic granites. Precambrian Res. 40–41, 509–541. https://doi.org/10.1016/0301-9268(88)90083-6.
Zhang, Y.-X., Tang, X.-C., Zhang, K.-J., Zeng, L., Gao, C.-L., 2014. U–Pb and Lu–Hf isotope systematics of detrital zircons from the Songpan–Ganzi Triassic flysch, NE Tibetan Plateau: implications for provenance and crustal growth. Int. Geol. Rev. 56, 29–56. https://doi.org/10.1080/00206814.2013.818754.